NAVAL POSTGRADUATE SCHOOL

MONTEREY, CALIFORNIA

THESIS

ASSESSING THE EFFECTS OF MULTI-NODE SENSOR NETWORK CONFIGURATIONS ON THE OPERATIONAL TEMPO

by

William M. Coleman

September 2014

Thesis Advisor: Phillip E. Pace
Co-Advisor: Edward L. Fisher

Approved for public release; distribution is unlimited

THIS PAGE INTENTIONALLY LEFT BLANK

REPORT DOCUMENTATION PAGE

Form Approved OMB No. 0704-0188

1. AGENCY USE ONLY *(Leave blank)*	**2. REPORT DATE** September 2014	**3. REPORT TYPE AND DATES COVERED** Master's Thesis

4. TITLE AND SUBTITLE
ASSESSING THE EFFECTS OF MULTI-NODE SENSOR NETWORK CONFIGURATIONS ON THE OPERATIONAL TEMPO

5. FUNDING NUMBERS

6. AUTHOR(S) William M. Coleman

7. PERFORMING ORGANIZATION NAME(S) AND ADDRESS(ES)
Center for Joint Services Electronic Warfare
Naval Postgraduate School
Monterey, CA 93943-5000

8. PERFORMING ORGANIZATION REPORT NUMBER

9. SPONSORING /MONITORING AGENCY NAME(S) AND ADDRESS(ES)
N/A

10. SPONSORING/MONITORING AGENCY REPORT NUMBER

11. SUPPLEMENTARY NOTES The views expressed in this thesis are those of the author and do not reflect the official policy or position of the Department of Defense or the U.S. Government. IRB Protocol number ____N/A____.

12a. DISTRIBUTION / AVAILABILITY STATEMENT
Approved for public release; distribution is unlimited

12b. DISTRIBUTION CODE
A

13. ABSTRACT (maximum 200 words)

The LPISimNet software tool provides the capability to quantify the performance of sensor network configurations by combining the information and physical domains. To combine the sensor network's performance in a coherent context with a decision-maker, Boyd's observe, orient, decide, act (OODA) loop is included along with its operational tempo.

This thesis develops a new version of LPISimNet (LPISimNet(V)3) by correcting a code error and including a network comparison file. Additionally, this thesis evaluates the effects of different network configurations and size on the maximum operational tempo. Simulation results for a static network indicate that as the network size increases the rate at which decisions can be made declines. A prediction for further decline is presented based on the simulations. Also, dynamic network simulation results for a three-, four-, five-, and six-node network display the importance of node placement and network geometry to help offset network degradation due to range fluctuation between nodes. By surrounding the dynamic nodes of the network with static nodes, the maximum operational tempo can be bounded between an upper and lower limit, stabilizing the decision-making speed. Finally, the effect of electronic attack on the operational tempo is presented to display the robustness of a network.

14. SUBJECT TERMS Sensor networks, OODA, wireless communication systems, characteristic tempo, operational tempo

15. NUMBER OF PAGES
107

16. PRICE CODE

17. SECURITY CLASSIFICATION OF REPORT	**18. SECURITY CLASSIFICATION OF THIS PAGE**	**19. SECURITY CLASSIFICATION OF ABSTRACT**	**20. LIMITATION OF ABSTRACT**
Unclassified	Unclassified	Unclassified	UU

NSN 7540-01-280-5500

Standard Form 298 (Rev. 2-89)
Prescribed by ANSI Std. 239-18

THIS PAGE INTENTIONALLY LEFT BLANK

Approved for public release; distribution is unlimited

ASSESSING THE EFFECTS OF MULTI-NODE SENSOR NETWORK CONFIGURATIONS ON THE OPERATIONAL TEMPO

William M. Coleman
Captain, United States Marine Corps
B.S., The Citadel, 2008

Submitted in partial fulfillment of the
requirements for the degree of

MASTER OF SCIENCE IN INFORMATION WARFARE SYSTEMS ENGINEERING

from the

NAVAL POSTGRADUATE SCHOOL
September 2014

Author: William M. Coleman

Approved by: Phillip E. Pace
Thesis Advisor

Edward L. Fisher
Co-Advisor

Dan C. Boger
Chair, Department of Information Sciences

THIS PAGE INTENTIONALLY LEFT BLANK

ABSTRACT

The LPISimNet software tool provides the capability to quantify the performance of sensor network configurations by combining the information and physical domains. To combine the sensor network's performance in a coherent context with a decision-maker, Boyd's observe, orient, decide, act (OODA) loop is included along with its operational tempo.

This thesis develops a new version of LPISimNet (LPISimNet(V)3) by correcting a code error and including a network comparison file. Additionally, this thesis evaluates the effects of different network configurations and size on the maximum operational tempo. Simulation results for a static network indicate that as the network size increases the rate at which decisions can be made declines. A prediction for further decline is presented based on the simulations. Also, dynamic network simulation results for a three-, four-, five-, and six-node network display the importance of node placement and network geometry to help offset network degradation due to range fluctuation between nodes. By surrounding the dynamic nodes of the network with static nodes, the maximum operational tempo can be bounded between an upper and lower limit, stabilizing the decision-making speed. Finally, the effect of electronic attack on the operational tempo is presented to display the robustness of a network.

THIS PAGE INTENTIONALLY LEFT BLANK

TABLE OF CONTENTS

LIST OF FIGURES

LIST OF TABLES

THIS PAGE INTENTIONALLY LEFT BLANK

LIST OF ACRONYMS AND ABBREVIATIONS

ASK	amplitude shift keying
ATC	air traffic control
B-FSK	binary frequency shift keying
B-PSK	binary phase shift keying
C2	command and control
ERP	effective radiated power
EW	electronic warfare
GUI	graphical user interface
HFT	high frequency trading
IEEE	Institute of Electrical and Electronics Engineering
MATLAB	Matrix Laboratory
MCDP	Marine Corps Doctrinal Publication
MCWP	Marine Corps Warfighting Publication
M-FSK	M-ary frequency shift keying
M-PSK	M-ary phase shift keying
M-QAM	M-ary quadrature amplitude modulation
NCW	network-centric warfare
OODA	observe, orient, decide, act
PAR	packet arrival rate
Q-PSK	quadrature phase shift keying
Rx	receiver
SAM	surface-to-air missile
SNR	signal-to-noise ratio
Tx	transmitter
UAV	unmanned aerial vehicle
WSN	wireless sensor network

THIS PAGE INTENTIONALLY LEFT BLANK

ACKNOWLEDGMENTS

First, I would like to thank my wonderful and caring wife, Heather. She has allowed me to devote a significant amount of time away from our family in order to complete my coursework and thesis. Her devotion to our family has allowed me to pursue this research and fulfill my goal of completing my degree.

Next, I would like to thank Professor Phillip Pace for his dedication to helping me complete my thesis as my advisor. He was able to point me in a direction to produce meaningful results. I will be forever grateful for his guidance, flexibility, devotion, mentorship, and support.

THIS PAGE INTENTIONALLY LEFT BLANK

I. INTRODUCTION

A. NETWORK-CENTRIC WARFARE AND THE INFORMATION ENVIRONMENT

The concept of network-centric warfare (NCW) was originally coined by Vice Admiral Arthur Cebrowski as his vision for the future of warfare [1]. His idea was that the military will change along with economics and technology [1]. With technological advances, the military is becoming more reliant on wireless networking to conduct operations. According to [2], the definition for NCW is "military operations that exploit state-of-the-art sensor information and networking technologies to integrate widely dispersed human decision makers, weapons, situational and targeting sensors and forces into a highly adaptive comprehensive system to achieve unprecedented mission effectiveness." The NCW concept is about networking different battlespace entities so the aggregate sum of all the force is working toward a common goal [3].

Military forces are already operating within the NCW construct, but a means to quantify the value of networking in the military domain can be done by viewing wireless sensor networks and autonomous systems through the lens of the information environment. According to [4], the information environment "is the aggregate of individuals, organizations, and systems that collect, process, disseminate, or act on information." The information environment is broken down into three dimensions: physical, informational, and cognitive [4]. The physical dimension consists of information systems and networks, a significant characteristic of the informational dimension is the content and flow of information, and specific characteristics of the cognitive dimension are awareness and decision-making [4]. With these characteristics in mind, wireless sensor networks fit into each dimension. The sensors and their wireless communication architecture are the physical aspects; the surveillance data and sharing of information throughout the network provides the content and flow; and the autonomous decision-making capability or the human-computer interface fulfills the requirement for the cognitive dimension.

As technological innovations improve, wireless sensor networks have evolved significantly. Sensor networks that are distributed provide a bridge to the physical world with one of the greatest benefits being the amount of information that can be passed throughout the network quickly to a decision-maker [5]. Previous work has illustrated how including the capability value K_μ within a generalized connectivity calculation can be used to measure the characteristic tempo of the network [6]. The generalized connectivity metric integrates the individual node capability values with their connections scaled by the length of the routes and reroutes (including their directionality) in order to measure the network's characteristic tempo λ_T [6]. Typically, the network is assumed to have a large (asymptotic) number of nodes each with the same capability value and to also assume that the network does not evolve in time [7]. However, if a traversed node on along a route has a low capability ($K_\mu << 1$) or a bottleneck, this route will not be able to maintain the full information flow capacity due to limited information exchange capabilities [8]. This limitation is accounted for in [8] with the *extended* generalized connectivity measure that accounts for the nodes with the lowest capability value.

Magalhaes et al. [7] discuss how only an arbitrary and subjective assignment of K_μ has been considered previously without regard to any network, data, or physical layer constraints and due to each node not having the same capability value it is imperative to account for them individually. By accounting for each node's capability value separately a more accurate representation of each node's capacity to maintain information flow through a distributed network is achieved [7]. These considerations were accounted for by including link properties between nodes such as bandwidth efficiency $B_{e\mu}$, data rate $R_{b\mu}$, and link margin J_μ [7].

To combine the network's characteristic tempo, data arrival rate (physical, information domains) in a coherent context with the decision-making tempo (cognitive domain), Boyd's OODA (observe, orient, decide, action) loop has been suggested in [6] along with its corresponding metric, the maximum operational tempo Λ_{OODA}. The utility of the OODA loop is the large number of applications it can be applied to. The

maximum operational tempo of the OODA loop combines the network's characteristic tempo, the decision making tempo and two action tempos that are a result of the decision-making [6]. Those capable of completing the loop with a higher operational tempo will have a higher performance [6]. By combining the dimensions of the information environment into network metrics, the quality of a network's information sharing and decision-making capabilities can be evaluated.

One problem associated with wireless sensor networks (WSN) is the degree of coverage the network achieves [9]. In theory, the more sensors employed in a WSN topology, the more coverage the network should have. The quality of service of wireless sensor networks is used to determine the minimum number of sensors required to achieve a specific level of coverage [9]. The idea is that no more sensors than necessary are employed. The coverage problem provides one reason for minimizing the number of sensors, but the result of degrading the operational tempo of a network due to the number of nodes employed is another.

Previous work shows how the combination of network metrics such as, node capability value, connectivity measure, network reach, network richness, and characteristic tempo can lead to generating the characteristic and maximum operational tempos of a network [6-8]. However, previous research has not focused on the negative ramifications of network size and configurations on the rate at which the network can complete an OODA loop. The importance of rapid decision making by computer networks can be seen in the practice of high frequency trading (HFT) in many of the stock exchanges around the world. Savani [10] defines HFT as "automated trading by computer programs that buy and sell stocks in trades that often last only second." The primary advantage of the companies that employ HFT is that through their technological advantage they are able to receive timely information about market products and act on this information before their competitors [10]. This is basically a computer system that is able to collect information from sensors and then act upon the knowledge generated from that information.

If the business world is adopting the concept of completing a decision-making process with their network faster than their competitors, then the concept should translate

into the military world as well. With the military relying on information systems that are connected via wireless links, the operational tempo of that network should be of upmost importance.

B. PRINCIPAL CONTRIBUTIONS

The results of this thesis are being compiled for submission in an article for *IEEE Transactions on Wireless Communications*. Due to not being intimately familiar with the MATLAB program that combines the network metrics at the outset of this research numerous hours were devoted to analyzing the program's code. Once the analysis was completed simulation setup began. At first, the simulation results indicated that an error existed in the code calculating the knowledge function. This error leads to a significant contribution, correcting the knowledge function calculation. Once the code correction was made, appropriate results were realized; specifically the knowledge function no longer produced negative values as it was allowed to previously. On top of the error correction a new network comparison file was added to the code to alleviate the time consuming process of data extraction that previously existed to compare networks. With the inclusion of the error correction and the network comparison file the simulation program is now known as LPISimNet(V)3.

Also, this thesis shows through simulations constructed in LPISimNet(V)3 that as the size of a wireless sensor network increases, the rate at which it can complete a decision-making cycle declines. Based on simulated results, a prediction of further performance degradation is presented to show the expected downward trend as the network size continues to increase. Although the degradation due to network size cannot be offset without node optimization, if dynamic sensors are employed, the degradation of network performance due to changing link distances can be offset through the proper placement of static nodes, or bracketing. These results highlight important factors that must be considered by the decision-makers planning for WSN operations in order to optimize the operational tempo of their network.

C. THESIS OUTLINE

This thesis is broken down into six chapters, which build upon the research conducted in [11] and [12]. Chapter II outlines network and adaptive node capability metrics, which form the baseline for the simulation model used to conduct analysis in this thesis. Chapter II provides the fundamental theory that leads to the generation of a networks ability to complete Boyd's decision-making cycle. Chapter III describes the simulation program called LPISimNet(V)2 produced in [12] that is a continuation of the program created in [11], which incorporates the network metrics from Chapter II. A description of the program flow, user interfaces, input requirements, and resulting products are presented. Additionally, Chapter III highlights difficulties encountered while using LPISimNet(V)2 and the error correction that was made to make the program more accurate, leading to the creation of LPISimNet(V)3. Chapter IV describes two different scenarios that were used to generate the preponderance of the results for this thesis. First, a static network scenario is presented along with the results produced from increasing the size of the network from two to nine nodes. Chapter IV also describes a dynamic scenario that increases from three to six nodes with the results of these four separate simulations, along with a method to offset network performance degradation due to range. Chapter V presents four additional considerations: the effect of electronic attack, the result of varying the command and control tempo of the network, the relationship between the signal-to-noise ratio and data throughput, and a new network comparison tool added into LPISimNet(V)3. Chapter VI provides the summary of the results along with recommendations for future research.

THIS PAGE INTENTIONALLY LEFT BLANK

II. NETWORK AND ADAPTIVE NODE CAPABILITY METRICS

A. INTRODUCTION

This chapter is focused on describing the network and adaptive node capability metrics that have been previously established. Adopting these metrics allows for leaders to assess the overall capability of a network to conduct information sharing and decision-making. This chapter presents these metrics to provide a general understanding for the analysis conducted in subsequent chapters.

Additionally, it is important to highlight the value added by each node throughout the network. In order to do this, an expansion has been made to the connectivity measure through the improvement to the adaptive node capability value K_{μ} [12]. The adaptive node capability value eliminates the assumption that all nodes in a network are equal, but are dictated by the link parameters between nodes, such as data rate, bandwidth efficiency and link margin [12]. This chapter first presents the network metrics that combine to form the operational tempo. Finally, the adaptive node capability value is presented.

B. NETWORKS METRICS

The primary metric to be used for evaluation is the maximum operational tempo Λ_{OODA}. However, for the convenience of the reader additional metrics that are needed to derive the maximum operational tempo are presented, to include: the connectivity measure C_M, network reach I_R, the network richness R_Q, and the networks characteristic tempo λ_T.

1. Generalized Connectivity Measure

Within a network, the generalized connectivity measure C_M is time-dependent and is represented by the sum of the individual node capability values scaled by the lengths of the connecting routes and the directionality of each node [6]. The generalized connectivity measure is expressed as [6]

$$C_M(t)=\sum_{\mu=1}^{N_T}K_\mu(t)\sum_{\nu=1}^{N_\mu}\sum_{\gamma=1}^{N_{\mu\nu}}L_\gamma^{\mu\nu}(d,t)=\sum_{\mu=1}^{N_T}K_\mu(t)\sum_{\nu=1}^{N_\mu}L^{\mu\nu}(t)\sum_{\gamma=1}^{N_{\mu\nu}}\frac{F_\gamma^{\mu\nu}(t)}{(d_\gamma)^{\xi}} \quad (1)$$

where N_T is the total number of nodes in the network, N_μ is the total number of nodes connected to node μ, $N_{\mu,\nu}$ is the total number of possible routes from node μ to node ν, d is the distance between nodes (or the number of links of the route γ), and $K_\mu(t)$ is the capability value of node μ, which relates to how quickly a node can process and disseminate information. $L_\gamma^{\mu\nu}$ is the information flow parameter for route γ between nodes μ and ν [6]. Both $K_\mu(t)$ and $L_\gamma^{\mu\nu}$ are bounded between zero and one $(0\le K_\mu(t), L_\gamma^{\mu\nu}\le 1)$ [6].

In order to simplify the generalized connectivity measure, it is assumed that K_μ is not time dependent and that any two nodes are either connected or not ($F_\gamma^{\mu\nu}(t)=0$ or 1) [6]. With this, the scaling exponent for the route length $\xi=1$, and the information flow parameter $L^{\mu\nu}=1$ are set as identical for each route [6]. With this result, (1) can be simplified to [2]

$$C_M(t)=\sum_{\mu=1}^{N_T}K_\mu\sum_{\nu=1}^{N_\mu}\sum_{\gamma=1}^{N_{\mu\nu}}\frac{F_\gamma^{\mu\nu}(t)}{d_\gamma}. \quad (2)$$

2. Reference Connectivity Measure

In order to establish a baseline network for comparison a reference network is defined as one with all nodes alike and each node is fully connected with each of the other nodes in the network, yielding $K_\mu=1$ and $F_\gamma^{\mu\nu}=1$ for all routes and nodes [6]. With this in mind, a reference connectivity measure (C_M^R) is defined as [6]

$$C_M^R=N_T(N_T-1)\left[1+\frac{(N_T-2)}{2}+\frac{(N_T-2)(N_T-3)}{2}\cdots\frac{(N_T-2)(N_T-3)\cdots 1}{N_T-1}\right]. \quad (3)$$

3. Network Reach

By normalizing the connectivity measure with the reference connectivity measure networks of the same size with different levels of connectivity, network configurations, and types of nodes can be compared [2, 6]. This normalization yields a dimensionless quantity called network reach I_R as [6]

$$I_R = \frac{C_M}{C_M^R}. \tag{4}$$

4. Network Richness

In order to develop the metric of network richness R_Q, the knowledge function $Q(R_{b\mu})$ must be defined. The knowledge function accounts for minimum data rates $R_{b\mu}^{\min}$ and the actual data rate $R_{b\mu}$ of each node throughout the network [6]. The minimum data rate $R_{b\mu}^{\min}$ is a value that is hardware specific, but represents the data rate for which information can be processed into useful knowledge [6]. From Shannon's information entropy theory, $Q(R_{b\mu})$ is defined as [6]

$$Q\left(R_{b\mu}\right) = \begin{cases} 0, & \text{if } R_{b\mu} < R_{b\mu}^{\min} \\ \ln\left(\dfrac{R_{b\mu}}{R_{b\mu}^{\min}}\right), & \text{if } R_{b\mu}^{\min} < R_{b\mu} < e \cdot R_{b\mu}^{\min} \\ \ln\left(\dfrac{e \cdot R_{b\mu}^{\min}}{R_{b\mu}^{\min}}\right) = 1, & \text{if } R_{b\mu} \geq e \cdot R_{b\mu}^{\min} \end{cases}. \tag{5}$$

By applying the knowledge function, the network richness is defined in [6] as the rate at which knowledge is generated within the network and represented as

$$R_Q = \frac{\sum_{\mu=1}^{N_T} R_{b\mu} Q\left(R_{b\mu}\right)}{N_T} \quad \text{Hz} \tag{6}$$

and shows, by inclusion of the knowledge function, that there is no way to share information at a greater rate than knowledge can be generated, and that if the data rate of the hardware is less than that of the minimum data rate required to generate knowledge, then no knowledge will be added by that node [2, 6].

5. Characteristic Tempo

Ling et al. [6] assert that every network has a defined information exchange rate that is limited by network topology, number of connections, types of equipment, etc. To evaluate these properties there are two assumptions proposed in [6]. The first assumption is "There is a Characteristic Tempo (λ_T), for information exchange associated with every network. It is primarily governed by the network topology and the information and communication technologies employed." The second assumption is "For every command and control (C2) structure and the associated doctrine and degree of training and professional mastery, there is a characteristic decision-making speed (λ_{C2})."

The characteristic tempo is defined as the product of the network reach and network richness as [6].

$$\lambda_T = I_R R_Q \quad \text{Hz} \tag{7}$$

The characteristic tempo measures the average rate at which knowledge can be generated and shared about the network [6].

6. Maximum Operational Tempo

In 1987, Colonel John Boyd presented *A Discourse on Winning and Losing* that developed the Observe, Orient, Decide, Act (OODA) loop to describe decision-making as a cycle. The application of the OODA loop is taught in many military doctrines, including [13] the United States Marine Corps Command and Control, Marine Corps Doctrinal Publication 6. Reference [13] uses the OODA loop to illustrate how the force that can complete the OODA loop more effectively than their enemy will consistently maintain the upper hand in conflict.

With this theory in mind [6] asserts that the OODA loop can be applied to a networked force as well. Figure 1 displays the OODA loop with specific time tempo parameters, where Δt_1 is the time between observation and orientation, which is governed by the characteristic tempo [2, 6]. The time between orientation and decision is defined as Δt_2, which is primarily a function of the decision-making speed [2, 6]. The time between decision and action is defined as Δt_3, which is not only a function of the characteristic tempo, but also the deployment speed λ_d, which is a physical aspect of the force [2, 6]. The final step, between the action and re-observation is defined as Δt_4, which is determined again by the characteristic tempo, but also the fighting tempo λ_f, which is also a physical property of the fighting force [2, 6]. Although the action tempos λ_d and λ_f are directly related to military applications, the OODA loop is not restricted to just military networks. Based on the concept of HFT, these action tempos do not necessarily have to be related to military force's actions, but could even involve businesses trading and purchasing stocks.

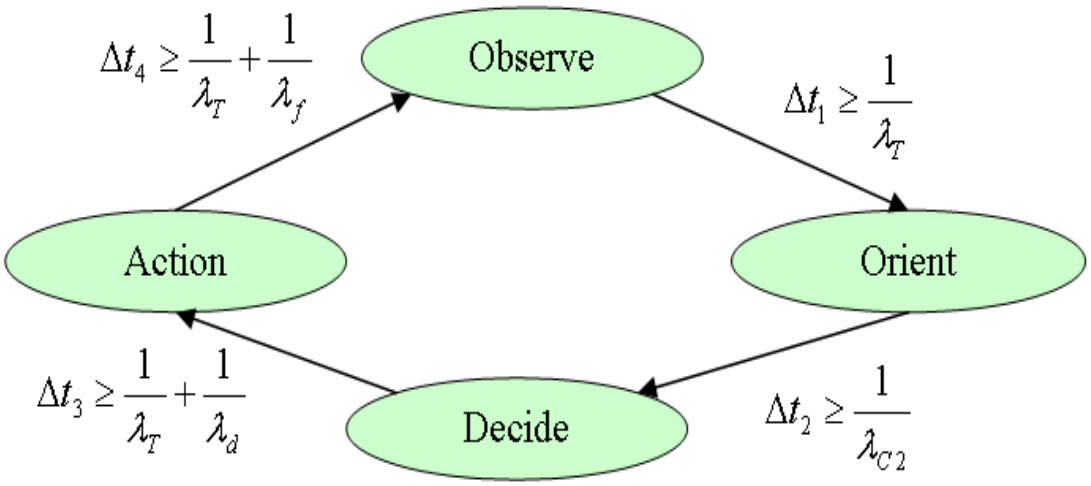

Figure 1. Time spent in each phase of the OODA loop, after [2]

By combining the timed parameters displayed in Figure 1 the maximum operational tempo Λ_{OODA} represents the maximum rate at which a network can complete the OODA loop and is defined as [2]

$$\Lambda_{OODA} \le \frac{1}{\left(\Delta t_1 + \Delta t_2 + \Delta t_3 + \Delta t_4\right)} \le \frac{\lambda_{C2}}{1 + \left(\frac{1}{\lambda_d} + \frac{1}{\lambda_f}\right)\lambda_{C2} + \frac{3\lambda_{C2}}{\lambda_T}} \quad \text{Hz.} \tag{8}$$

C. EXTENDED GENERALIZED CONNECTIVITY MEASURE

Although the generalized connectivity measure was previously developed, it did not take into account the possibility of bottleneck nodes. The extended generalized connectivity measure developed in [8, 11] takes into account that a time dependent flow coefficient $F_\gamma^{\mu\nu}$ and the instance where there is only partial efficiency in one of the network routes. As an example, if a traversed node ν on a connected route γ has a capability value $K_\mu << 1$, then this route will not continue to maintain the full capacity of information flow [8]. Taking this specific limitation into account, the extended generalized connectivity measure is [8, 11]

$$C_M(t) = \sum_{\mu=1}^{N_T} \sum_{\nu=1}^{N_\mu} \sum_{\gamma=1}^{N_{\mu\nu}} \frac{K_\gamma F_\gamma^{\mu\nu}}{d_\gamma} \tag{9}$$

where K_γ reflects the node with the lowest capability value (or bottleneck) in route γ. Note the fact that K_γ in the route only considers the transmitting and exchanging nodes and not the receivers [8]. This consideration is due to the fact that nodes often accept information without the same information processing capability required to transmit [8]. As an example, in route 1 → 3 → 2, only the transmitter (node 1) and exchanger (node 3) are available for assignment to K_γ, which represents the bottleneck of the information flow [8].

D. ADAPTIVE NODE CAPABILITY METRIC

A node's capability is defined as the ability of the node to transmit and process information quickly [2]. Although this is the case, the capability of a node is often dependent on the bandwidth of its transmission channel and the power available to each node [12]. The metrics described in [6] accounted for the node capability value, but did not consider the specific link characteristics between nodes. The K_μ values were originally assumed to have the same values [7]. With this being the case [12] proposed an extended definition of node capability as "a measure of the amount of data one node can process and transmit, and how efficient this node is in terms of power and bandwidth, in order to make the information both detectable and understandable to the next node and the network as a whole." In order to build the proposed node capability value the contributing components were defined in [7, 12] as data rate (or throughput), bandwidth efficiency, and link margin.

1. Data Rate

The first condition for the proposed model in [12] was determining the channel quality between two nodes in a network. The channel quality is dictated by the signal quality between nodes, commonly known as the signal-to-noise ratio (SNR) [12]. The SNR in dB is defined as [12]

$$SNR(t) = P_r(dBW) - P_n(dBW) - L_i(dB) \quad \text{dB} \tag{10}$$

where t is the time index, P_r is the received power at the receiver, P_n is the noise power of the receiver, and L_i is the implementation loss of the receiver due to hardware manufacturing.

The received power of an antenna can be defined as a function of transmitted power P_t (in dBW), the transmit antenna gain G_t (in dB), the receiving antenna gain G_r (in dB), and the line-of-sight path loss L_p (in dB) [12]. The received power in dBW is expressed as [12]

$$P_r = P_t + G_t + G_r - L_p \quad \text{dBW}. \tag{11}$$

In order to calculate the line-of-sight path loss in dB the distance between the transmitter and receiver in kilometers d_{km} and the transmitted frequency in MHz f_{MHz} are used as [12]

$$L_p(t) = 32.44 + 20\log(f_{MHz}) + 20\log(d_{km}) \quad \text{dB}. \tag{12}$$

Due to dynamic scenarios (scenarios involving moving nodes), the distances between nodes can vary, therefore the line-of-sight path loss is time dependent [12].

The receiver's noise power is a function of thermal noise and the noise factor F_n of the receiver [12]. Using these two parameters, the noise power is expressed as [12]

$$P_n = 10\log(kTF_nB) \quad \text{dBW} \tag{13}$$

where k is Boltzmann's constant $1.38e-21\,J/K$, T is temperature in Kelvin (290 K), with $kT = 4e-21$ W/Hz, and B is the bandwidth of the receiver in Hz.

Typically, the minimum required SNR to overcome multipath is 13 dB or greater [12]. After the SNR at a receiving node is calculated due to a specific transmitter, it is possible to determine the packet loss rate ξ_r while assuming a fixed packet error rate P_0 [12]. In order to determine the probability of dropping a packet P_d and ξ_r as a function of P_0, the SNR values were extrapolated from $17 \le SNR \le 22$ dB in [14, 15] to provide a wider SNR range of $13 \le SNR \le 25$ dB in [12]. Figure 2 shows the relationship between P_d and ξ_r as SNR changes in one dB steps.

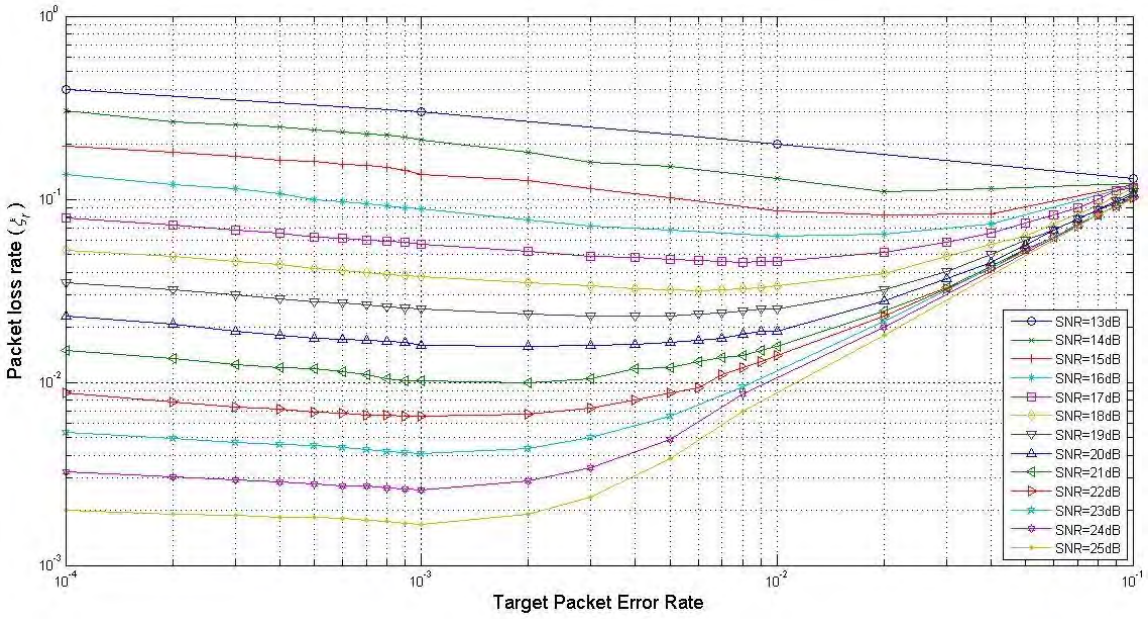

Figure 2. Packet loss rate and packet error rate for different SNR, from [12]

Once ξ_r and P_0 are determined from Figure 2, the probability of dropping a packet is determined as [12]

$$P_d(t) = \frac{[\xi_r(t) - P_0]}{(1 - P_0)}. \tag{14}$$

The time dependent throughput η is defined next, and is dependent on P_d and P_0 [12]. From [14, 15], throughput is defined as

$$\eta(t) = \lambda T_f (1 - P_d)(1 - P_0) \tag{15}$$

where λ is the packet arrival rate and T_f is the frame time. The product λT_f is assumed to be fixed, but is the average packet arrival rate entering the queue [7]. The throughput value represents the average number of packets which pass through a frame at a given time, and has a strong dependency on SNR [12].

Finally, given the throughput, it is possible to determine the data rate $R_{b\mu}$ delivered to each nodes receiver. The data rate is a function of fixed values of packet length N_b, throughput η, and frame time T_f, and is expressed as [7]

$$R_{b\mu}(t) = \left| \frac{\eta(t)}{T_f} \right| N_b \quad \text{bps.} \tag{16}$$

Due to the numerous modulation schemes able to be employed in communications systems, the maximum transmission data rate a node can support is bounded by an upper limit [7, 12]. Table 1 provides examples of the upper limits for the normal IEEE standard (802.X) active groups.

Table 1. Comparison of IEEE 802 standards, from [12]

Standard	Frequency	Data Rate	Modulation Methods
802.11	2.4 GHz	2 Mbps	Q-PSK
802.11a	5 GHz	6 and 9 Mbps	B-PSK
		12 and 18 Mbps	Q-PSK
		24 and 36 Mbps	16-QAM
		48 and 54 Mbps	64-QAM
802.11g	2.4 GHz	6 and 9 Mbps	B-PSK
		12 and 18 Mbps	Q-PSK
		24 and 36 Mbps	16-QAM
		48 and 54 Mbps	64-QAM
802.16	2 GHz to 11 GHz	100 Mbps (peak)	B-PSK, Q-PSK, 16/64/256-QAM

2. Bandwidth Efficiency

The next parameter to be defined is the bandwidth efficiency. Reference [12] assumes that a node can transmit using one of the following modulation schemes:

- B-PSK (binary phase shift keying)
- Q-PSK (quadrature phase shift keying)
- M-PSK (M-ary phase shift keying)
- M-QAM (M-ary quadrature amplitude modulation)
- M-FSK (M-ary frequency shift keying)

- B-FSK (binary frequency shift keying)
- ASK (amplitude shift keying)

The bandwidth efficiency $B_{e\mu}$ quantifies the abilities of each modulation scheme to operate within a limited transmission bandwidth [12]. The bandwidth efficiency $B_{e\mu}$ is defined as the ratio of the transmission data rate $R_{b\mu}$ and the transmission bandwidth B_T and is expressed as [7, 12]

$$B_{e\mu}(t) = \frac{R_{b\mu}(t)}{B_T} \quad \text{bps/Hz.} \tag{17}$$

The transmission bandwidth B_T is dependent on the modulation scheme being employed and represents the minimum bandwidth that is necessary for transmission [7, 12]. The required B_T for each modulation scheme is reflected in Table 2.

Table 2. B_T for each modulation scheme, from [12]

Modulation schemes	**Transmission bandwidth (Hz)**
B-PSK	$B_T = (1+r')R_{b\mu}$
Q-PSK	$B_T = \frac{(1+r')R_{b\mu}}{2}$
M-PSK	$B_T = \left(\frac{1+r'}{\log_2(M)}\right)R_{b\mu}$
M-QAM	$B_T = \left(\frac{1+r'}{\log_2(M)}\right)R_{b\mu}$
M-FSK	$B_T = \left[\frac{(1+r')M}{\log_2(M)}\right]R_{b\mu}$
B-FSK	$B_T = (1+r')R_{b\mu}$
ASK	$B_T = (1+r')R_{b\mu}$

The transmission bandwidth expressions in Table 2 are functions of the pulse shaping filter r' and the number of signal element combinations M. For the purposes of this thesis, a value of $r' = 0.5$ is used, which represents the raised cosine filter. The variable M, which is shown in the equations for M-PSK, M-QAM, and M-FSK is expressed as $M = 2^L$, where L is the number of bits controlling the signal levels, typically $L = 2,...,8$ with $L = 1$ defining B-PSK [12]. Table 3 shows $B_{e\mu}$ for different values of M at $r' = 0.5$ when considering multi-level ASK, PSK, and FSK.

Table 3. $B_{e\mu}$ for typical digital-to-analog modulations, after [12]

	$r' = 0.5$
ASK	0.667
4-PSK	1.333
8-PSK	2
16-PSK	2.667
64-PSK	4
4-FSK	0.333
8-FSK	0.25
16-FSK	0.1667
64-FSK	0.0625

3. Link Margin

Although the bandwidth efficiency is an important parameter needed to evaluate the node capability the link margin between connected nodes is equally important [12]. In order to formulate the link margin between nodes the *required* energy per bit to noise power density per hertz $[E_b / N_o]_{req}$ is needed. The *required* energy per bit to noise

power density is a function of the desired probability of bit error P_b and M [12]. Table 4 provides the equations for $[E_b / N_o]_{req}$, which were shown in [12] and later used in its model. The $[E_b / N_o]_{req}$ equations in Table 4 are a function of P_b, which represents the required probability of bit error at the receiver, and should not be confused with P_0 which is the target packet error rate [12].

Table 4. $[E_b / N_o]_{req}$ for typical modulation schemes, from [12]

Modulation schemes	$\left[E_b / N_o\right]_{req}$
B-PSK	$\left[\frac{E_b}{N_o}\right]_{req} = \frac{\left[Q^{-1}\left(P_b\right)\right]^2}{2}$
Q-PSK	$\left[\frac{E_b}{N_o}\right]_{req} = \frac{\left[Q^{-1}\left(P_b\right)\right]^2}{2}$
M-PSK	$\left[\frac{E_b}{N_o}\right]_{req} = \frac{\left[Q^{-1}\left(\frac{P_b \log_2(M)}{2}\right)\right]^2}{2\left[\log_2(M)\right]\left[\sin^2\left(\frac{\pi}{M}\right)\right]}$
M-QAM	$\left[\frac{E_b}{N_o}\right]_{req} = \left[\frac{M-1}{3\log_2(M)}\right]\left[Q^{-1}\left(\frac{P_b \log_2(M)}{4\left[1-\left(1/\sqrt{M}\right)\right]}\right)\right]^2$
M-FSK	$\left[\frac{E_b}{N_o}\right]_{req} = \frac{\left[Q^{-1}\left(\frac{2P_b}{M}\right)\right]^2}{\log_2(M)}$
B-FSK	$\left\lfloor\frac{E_b}{N_o}\right\rfloor_{req} = \left[Q^{-1}\left(P_b\right)\right]^2$
ASK	$\left\lfloor\frac{E_b}{N_o}\right\rfloor_{req} = \left[Q^{-1}\left(P_b\right)\right]^2$

The *actual* received energy per bit to noise power density $[E_b / N_o]_r$ is defined at the input of the receiver and determines the required performance of the receiver is achieved [12]. The received energy per noise power spectral density is defined as [7, 12]

$$\left\lfloor \frac{E_b}{N_o} \right\rfloor_r (\text{dB}) = SNR(\text{dB}) - B_{e\mu} \text{ (dBbps/Hz)}. \tag{18}$$

Subtracting the required from the received energy per noise power spectral density, the link margin J_μ for node μ is [16]

$$J_\mu(t) = \left\lfloor \frac{E_b}{N_o} \right\rfloor_r (\text{dB}) - \left\lfloor \frac{E_b}{N_o} \right\rfloor_{req} (\text{dB}). \tag{19}$$

Now that all the individual metrics have been defined, the adaptive node capability value in [7, 12] can be addressed.

4. Adaptive Node Capability Value

Based on the definitions of the data rate, bandwidth efficiency, and link margin the node capability value K_μ is defined as [7, 12]

$$K_\mu(t) = R_{b\mu}(t) B_{e\mu} J_\mu(t). \tag{20}$$

In (20) it is assumed that each variable is independent of one another [12]. Because more than one node can be connected to any other node, the node capability value must take into account the average value of all links γ from node μ to node ν [12]. The node capability value should only be affected by those nodes which are directly connected to node μ [12]. In order to account for this, the average over N_μ attached links is computed as [7, 12]

$$\overline{K}_\mu(t) = \frac{1}{N_\mu} \sum_{i=1}^{N_\mu} \{[R_{b\mu}(t)] B_{e\mu}[J_\mu(t)]\} \tag{21}$$

where $\overline{K}_\mu$ is the average value.

In order to overcome the throughput limitations of $R_{b\mu}$ and to consider that $0 \le K_\mu \le 1$ as used by the generalized connectivity measure, the capability value is normalized by the highest possible average node capability value [7, 12]. The normalized node capability value is expressed as [7, 12]

$$\overline{K}_\mu^N(t) = \frac{\frac{1}{N_\mu}\sum_{i=1}^{N_\mu}\{[R_{b\mu}(t)]B_{e\mu}[J_\mu(t)]\}}{\max[\overline{K}_\mu(t)]} \tag{22}$$

where the maximum is taken over all nodes N_T.

Figure 3 provides as a graphical representation of such requirements. It shows three nodes. However, the node capability value of node μ_1 is calculated using only the nodes directly connected to it, μ_2 to μ_i.

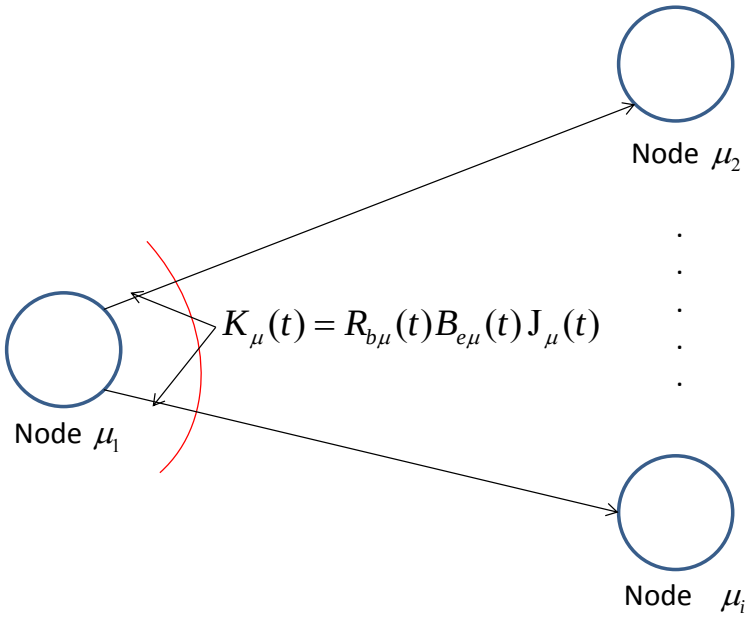

Figure 3. Node capability value affected only by directly connected nodes

E. CONCLUSION

This chapter provides baseline information for the model developed in [6] and extended by [8, 11] and [7, 12], which will be used to conduct additional analysis. The network metrics tied to Boyd's OODA loop provide background knowledge for the characteristic tempo and maximum operational tempo analysis to follow. Additionally, the adaptive node capability metric and its supporting parameters provide the theory for the node capability analysis along with its contribution to the network metrics. The next chapter is dedicated to summarizing the simulation tool developed in [12] along with inherent difficulties that were encountered when using the simulation program and the corrections and improvements that were made to correct the error identified that results in the new version, LPISimNet(V)3.

III. MODELING PROGRAM DESCRIPTION

A. INTRODUCTION

The Matrix Laboratory (MATLAB) program known as LPISimNet(V)1 was originally developed in [11] and was improved upon in [12] (LPISimNet(V)2) in order to calculate key performance metrics of a sensor-network simulation. The program was originally designed to calculate the metrics for an individual network. However, this thesis modified the program to compare multiple networks and account for code corrections yielding LPISimNet(V)3. This is significant since network enabled electronic warfare techniques are often used to attack surface-to-air missile (SAM) systems which in addition to using a low probability of intercept emitter are also network enabled.

In order to understand how LPISimNet(V)3 was used to conduct the analysis a brief discussion on how the program functions is provided. First described is the flow of the MATLAB program, including figures to provide a visual representation of the user interface. Next, limitations and difficulties in using LPISimNet(V)2 are presented, as well as corrections, yielding LPISimNet(V)3, that were made to ensure that the simulation results are accurate. Lastly, a conclusion is provided to highlight important discussions from this chapter.

B. PROGRAM FLOW

The MATLAB program, LPISimNet(V)3, consists of numerous connecting files which make up the overall program. Corrections to LPISimNet(V)2 then resulted in LPISimNet(V)3 which is used to produce the results shown in this thesis. After the additions made in [12], LPISimNet(V)3 includes a total of 12 different files:

- Calculator.m
- CalculatorKu.m
- Cos.m
- Legend.fig
- Legend.m

- PainterEditor.m
- PaintViewer.m
- ScenarioEditor.fig
- ScenarioEditor.m
- SimulationViewer.fig
- SimulationViewer.m
- Xi_vs_P02.mat

In order for the program to run, all of these files must be within the same folder accessible by MATLAB. The general flow starts with the ScenarioEditor.m, which when run provides the user with a graphical user interface (GUI) to load the network parameters. Figure 4 provides an example of the Scenario Editor GUI at one time index. The Scenario Editor is broken down into three major fields; top level properties, node properties, and graphical representation with a 2-D grid being measured in kilometers (e.g., height versus range, range versus cross-range, etc.).

Figure 4 shows the network parameters input locations on the left side of the image. The top level properties include the number of nodes, number of time indexes, and action tempos; decision tempo λ_{C2}, deployment tempo λ_d, and fighting tempo λ_f. These action tempos are constant throughout each scenario and for the simulations conducted in this thesis these values were kept at the baseline using medium-action tempos.

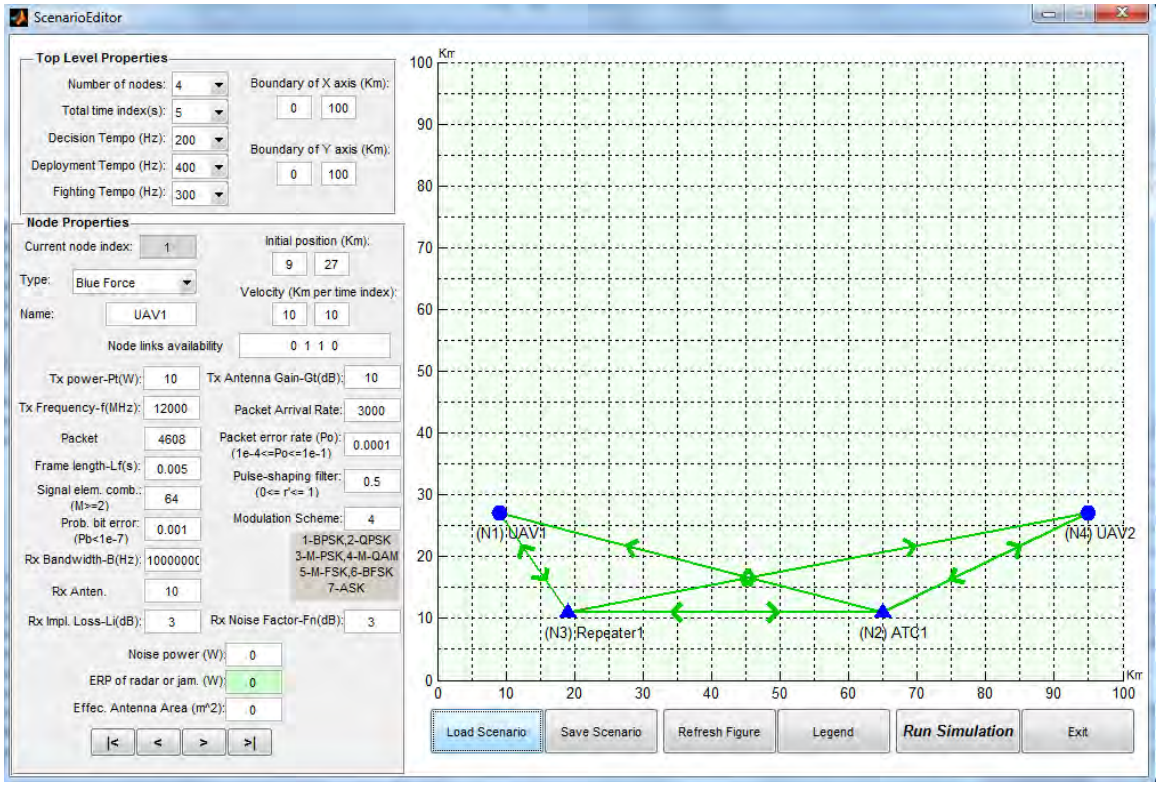

Figure 4. ScenarioEditor.fig example from LPISimNet(V)3

Changing the action tempos within the Scenario Editor causes varying effects on the maximum operational tempo of the network. LPISimNet(V)3 allows for the values of these action tempos to range from 100 Hz to 900 Hz. The medium-action tempo sets these values at 200 Hz, 400 Hz, and 300 Hz for λ_{C2}, λ_d, and λ_f, respectively, as defined in [12]. Figure 5 is provided to show a graphical representation of the effects of varying action tempos on the maximum operational tempo. The variation of the action tempos is first analyzed in [12] to show how the differing interactions of action tempos cause the maximum operational tempo to change. The y-axis is the action tempo in Hz which is input into the top-level properties panel. The x-axis is Λ_{OODA} for each interaction as the action tempos increase from 100 Hz to 900 Hz independently. The medium-action tempos are the only location where the differing action tempos align on the Λ_{OODA} axis. The results in Figure 5 show that the action tempo which causes the greatest change in Λ_{OODA} is λ_{C2}.

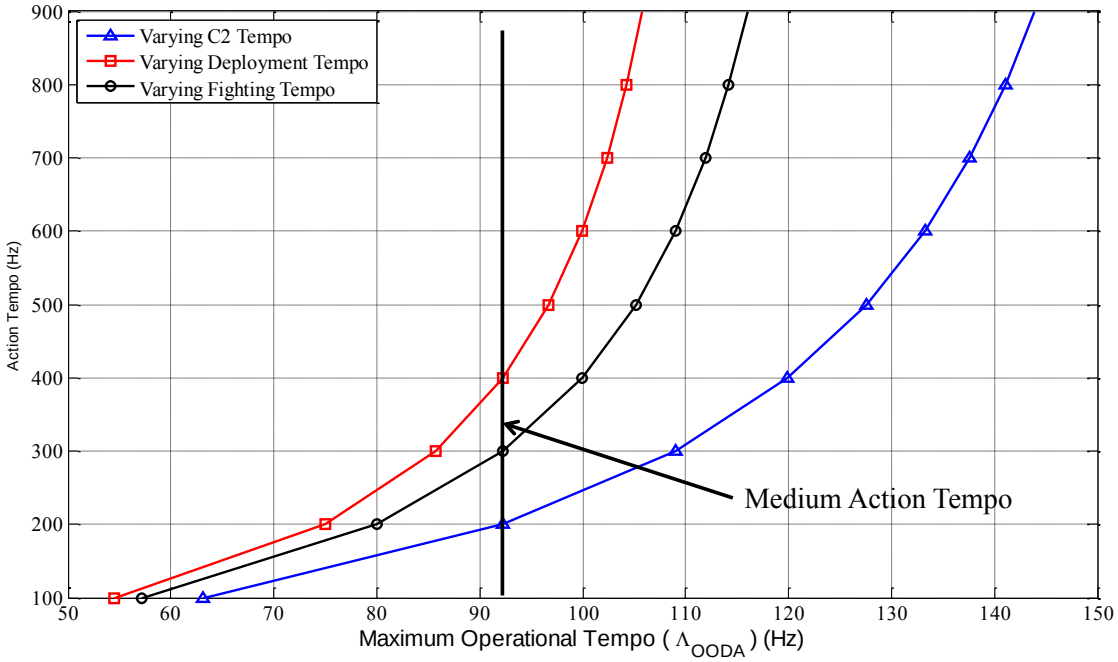

Figure 5. Example of action tempos effecting maximum operational tempo

Once the top-level properties are assigned within the Scenario Editor the specific node parameters are assigned. The node parameters include:

- Type of node (Blue Force, Hostile Jammer, or Radar Target)
- Initial position (x and y coordinates in km)
- Name (specified by the user)
- Velocity (km per time index)
- Node links available (the communication links between nodes, represented by 1 if the link is available and 0 if no link is available)
- Transmit Power (Watts)
- Transmit Antenna Gain (dB)
- Transmit Frequency (MHz)
- Packet Arrival Rate
- Packet Length

- Frame Length (seconds)
- Packet error rate
- Signal element combinations
- Probability of bit error
- Modulation Scheme
- Receiver Bandwidth (Hz)
- Receive Antenna Gain (dB)
- Receiver Implementation Loss (dB)
- Receiver Noise Factor (dB)

Additional properties can be assigned if radars and/or jammers are being simulated. These properties include noise power in Watts, effective radiated power (ERP) of the radar or jammer in Watts, and the effective antenna area in square meters.

The left and right arrows at the bottom of Figure 4 allow the user to toggle between nodes in order to assign different properties, while the top level properties are common to each node. After all parameters are assigned the scenario can either be saved, or run by clicking on save scenario or run simulation, respectively.

After run simulation is selected, the program first calls CalculatorKu.m, which calculates all the node capability metrics and saves them to Node_Cap.mat. Next, it calls Calculator.m, which will then calculate all the network metrics. Once the simulation has completed its calculations the user is prompted to save the simulation so it can be opened by the Simulation Viewer.

The Simulation Viewer is another GUI, which is opened by running SimulationViewer.m. The Simulation Viewer allows the user to visually see the results of the simulation for an individual network. Figure 6 is provided as an example view of what the Simulation Viewer produces at a single time index.

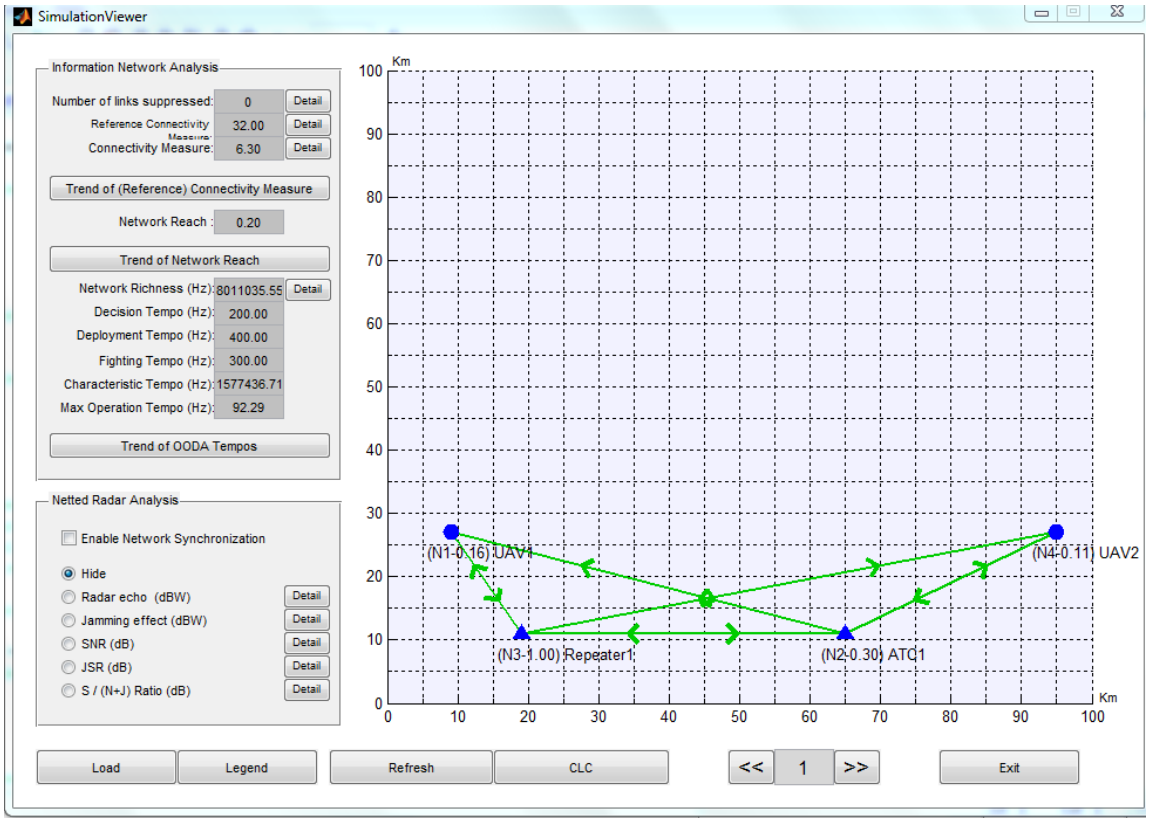

Figure 6. SimulationViewer.fig example from LPISimNet(V)3

The SimulationViewer.fig output provides the user with the interface to conduct analysis on the specific network metrics calculated by LPISimNet(V)3. The network metrics include reference connectivity measure C_M^R, connectivity measure C_M, network reach I_R, network richness R_Q, characteristic tempo λ_T, and maximum operational tempo Λ_{OODA}. The individual node capability values are displayed next to each node in the grid panel. If the scenario includes moving nodes over multiple time indexes, the arrows at the bottom of the figure allow for the user to toggle between each time index, which changes the values of the node capabilities on the figure for each node, as well as the network metrics displayed in the Information Network Analysis panel of the figure.

C. LIMITATIONS AND IMPROVEMENTS LEADING TO LPISIMNET(V)3

The MATLAB program, LPISimNet(V)2, developed in [12] is a powerful network simulation program. It enables the user to model realistic sensor and

communication networks, compute network and node capability metrics, provides a user friendly GUI, and a means to store simulation results. Although the program provides these capabilities, there are inherent difficulties with using the program to include network comparison and computation time. Additionally an error was found in the code, which initially caused inaccurate simulation results.

1. Data Collection Shortfalls

Due to not being intimately familiar with the program at the outset of this research numerous hours were devoted to analyzing the MATLAB code which makes up LPISimNet(V)2. Once this analysis was completed the simulation setup began. At the beginning of setting up numerous simulations it was noticed that the program was hard to use to compare networks. The program only allows the user to view one set of simulation results at a time. From a practical standpoint, this makes it hard for a decision-maker to make a quick decision about the optimal topology. In order to conduct a network comparison, data has to be manually extracted from the simulation results, placed into Microsoft Excel, and then read back into MATLAB to plot multiple network metrics on the same figure. This is a time consuming process, which in the military will not be tolerated due to having to make decisions in a time constrained environment. In order to mitigate this time consuming process a network comparison file was added to LPISimNet(V)3 which enables the user to view both static and dynamic results of multiple networks on the same figures. Example results are provided in Chapter V of this thesis.

2. Computation Time

Even though extracting the data is time consuming, the time required for the program to compute valuable network metrics for networks greater than seven nodes is extremely high. For example, a seven node network takes approximately 20 minutes to complete a simulation. When the network size is increased to eight nodes, the simulation takes approximately seven hours to complete. Finally, when the network size is increased to nine nodes, the simulation requires more than nine days to compute all the network metrics. The simulations up to eight nodes were run using a laptop computer

with a CORE i7 processor with 8 GB of RAM. Due to 22.6 GB of RAM required for the nine node simulation a desktop computer with a quad-core processor and 24 GB of RAM was used. Sensor and communication networks often employ many more than nine nodes. With that being the case, the computational burden carried forward into LPISimNet(V)3 must be reduced in order to make it a more useful tool for modeling. The computational speed of the program could potentially be reduced by incorporating parallel processing into the programming.

3. Error Corrections

Once the scenarios were designed, the simulations were started. The initial results produced erroneous results, which included negative values for the knowledge function and network richness. Based on the way these metrics were defined in Chapter II, negative results should be impossible to achieve. This error was due to a code error when computing the knowledge function as described by equation (5). If the data rate $R_{b\mu}$ is less than the minimum data rate $R_{b\mu}^{\min}$ then the knowledge function should be zero, which means the node is not providing any information to the network [6]. Additionally, if $R_{b\mu}$ is greater than $e \cdot R_{b\mu}^{\min}$ then information is being disseminated faster than knowledge can be generated, therefore the knowledge function should be one [6]. In the original LPISimNet(V)2 code, the knowledge function did not allow for this bounding to occur. This error caused a cascading effect on additional metrics which are ultimately depended on the knowledge function's accuracy.

With the knowledge function allowing negative values, the network richness was reduced, which causes the characteristic tempo to be lower than it should be or negative. A major contribution to the LPISimNet software is a correction to the code to bind the knowledge function between zero and one. This ultimately yields a more accurate simulation of the networks performance and aligns the code with the definition of the metrics. The Appendix to this thesis provides the details of the code correction for the knowledge function.

D. CONCLUSION

This chapter provided an overview of the modeling tool, originally created in [11], enhanced in [12], and corrected in this thesis. The GUI descriptions were provided in order to describe how a user would input data and receive the output of the simulation results. Finally, the limitations and corrections made creating LPISimNet(V)3 were presented. The next chapter is devoted to describing the scenarios used to conduct simulations along with their results.

THIS PAGE INTENTIONALLY LEFT BLANK

IV. SIMULATIONS

A. INTRODUCTION

The results in [11] and [12] are used to show how their respective models worked and validate the relationships between different metrics. Although those results are generated, they do not explore the effects of the size of the network configurations or compare multiple networks against each other. This thesis explores the effects of different network configurations on the key network performance metrics incorporated in the new model. Also, the degradation in network performance due to range is examined. A key performance metric investigated is the maximum operational tempo, and how increasing the number of nodes within a sensor or communications network affects the overall performance, as well as a method to offset the network performance degradation due to range.

This chapter incorporates two separate scenarios, one static (stationary nodes) and one dynamic (moving nodes). It first describes the static scenario and its size is increased from two to nine nodes, followed by the effects on the maximum operational tempo as the network size increases. Next, the dynamic scenario is described, to include the build up from three to six nodes, which in the end includes two dynamic and four stationary nodes. After the dynamic scenario description, detailed analysis on the node capability values, characteristic tempo, and maximum operational tempo is provided. Finally, a conclusion section is included to highlight the key findings of the simulation results.

B. STATIC SCENARIO

1. Scenario Setup

Static sensor networks are used in both military and business environments. The United States Marine Corps employs unattended ground sensors to detect vehicle and foot traffic in remote locations [17]. Additionally, static sensors are used in industrial settings to detect the level of liquid in a tank or to detect motion between the aisles of a warehouse. With this in mind, a static network was created following Richard Kershner's method to cover a region with disks. Kershner [18] describes the best method

for covering an area with disks is by placing their center points in an equilateral triangular network. Wireless network lessons at Ohio State University refer to Kershner's method as a basic means to distribute nodes within a wireless network. Although in [19] they do not distribute nodes as specifically stated in Kershner's method, they use it as a baseline for how to model their network's coverage. Figure 7 provides an example of how Kershner would cover a set with circular disks.

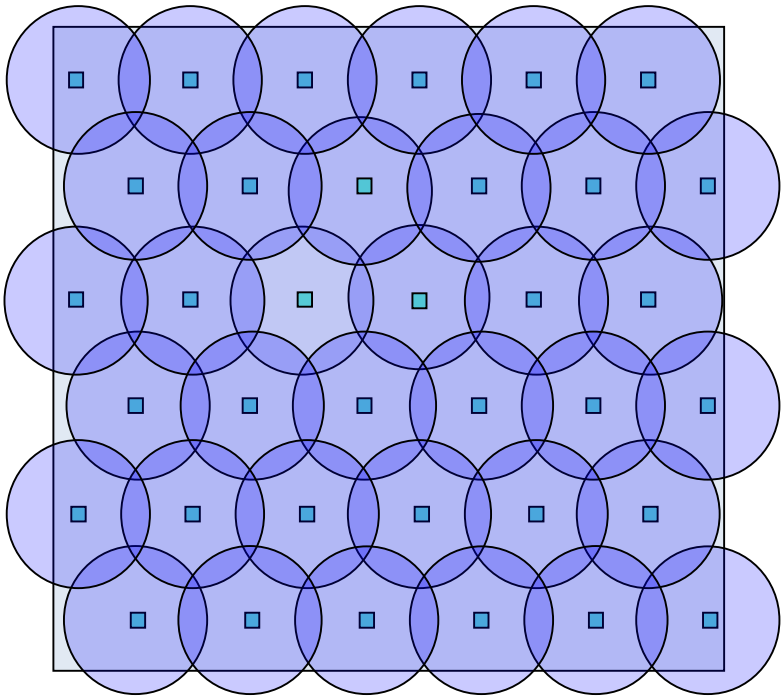

Figure 7. Example of Kershner's method to cover a region, after [19]

Although the static network created for this thesis is not concerned with covering a region, the node placement followed the triangular lattice pattern described in [18]. The static network is designed to increase from two to nine nodes in order to show the effects of network size on the maximum operational tempo, or the rate at which the network can complete an entire OODA loop. All nodes in the network have the exact same parameters with the exception of their location. Table 5 provides a summary of the transmit and receive parameters used for each node in the scenario. Due to the way LPISimNet(V)3 is designed, three top level tempos were required to be assigned,

command and control tempo λ_{C2}, deployment tempo λ_d, and fighting tempo λ_f, which are assigned the values of 200 Hz, 400 Hz, and 300 Hz, respectively, as in [12]. These specific tempos do not affect the trend to be displayed. However, by changing any one of them at the start of any simulation will yield different maximum operational tempo result.

Table 5. Summary of static network node parameters

Name	**N1-N8**
Type	Friendly
Velocity (km/time index)	(0,0)
Transmitted Power (W)	10
Transmitted Antenna Gain (dB)	20
Transmitted Frequency (GHz)	14
Packet Arrival Rate (packets/s)	3000
Packet Length (bits)	4608
Frame Length (ms)	5
Packet Error Rate	10^{-4}
Modulation Scheme	B-PSK
Maximum data rate allowed (Mbps)	6
Signal Element Combinations	2
Raised Cosine Filter Factor	0.5
Probability of Bit Error - Rx	10^{-3}
Receiver Bandwidth (MHz)	10
Antenna Gain (dB)	15
Noise Factor - Rx	3
Implementation Loss	10

Figures 8 and 9 are provided to show how the network geometry changes as the number of nodes increases from two to nine. Figure 8 provides a graphical representation for the three-node network and Figure 9 displays the network layout for the nine-node network. The axis grids are measured in kilometers. The green lines in the figures reflect the communication links between the nodes, with the arrows representing the direction of transmission between the nodes. The node numbers are indicated by the labels next to each node. It is important to note that not every node is fully connected.

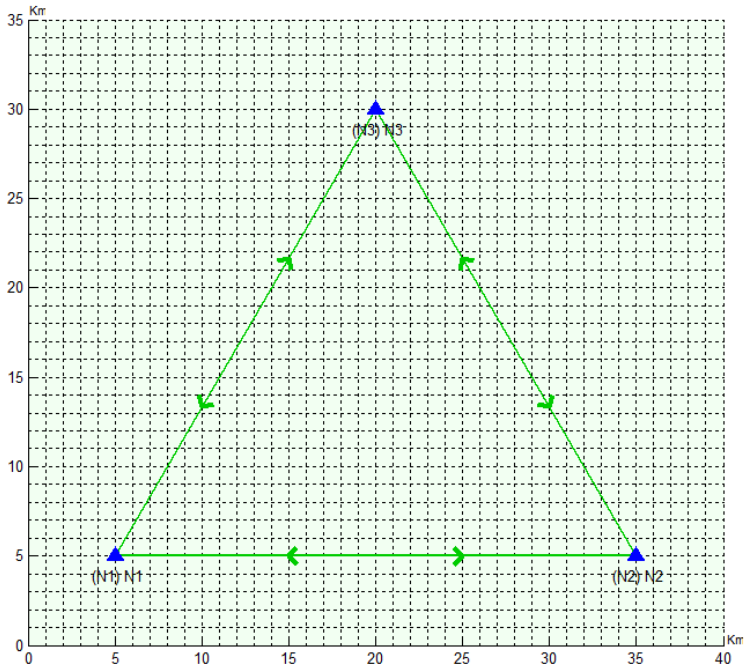

Figure 8. LPISimNet(V)3 snapshot of three-node static network geometry

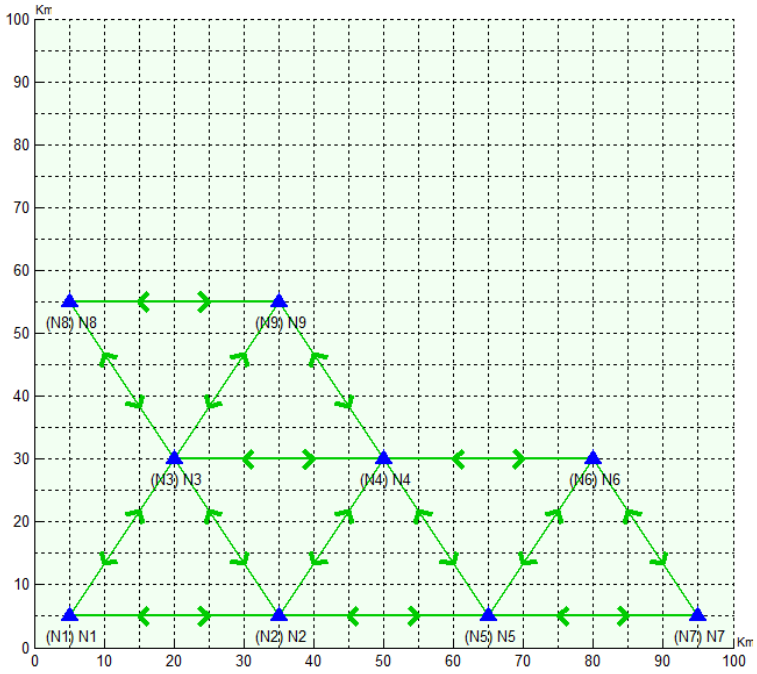

Figure 9. LPISimNet(V)3 snapshot of nine-node static network geometry

Each node in the network represents a sensor on the ground. The sensors could be used to detect ground movement, seismic activity, or conduct target location. The overall

goal is to show how the size of the network dictates the rate at which the network can share and exchange information which can be used to conduct decision-making. The next section is devoted to discussing the effects of such network expansion on the operational capability.

2. Results

It is intuitive to think that having more sensors would be beneficial for information collection and coverage. However, there are implications to having a large network. Figure 10 shows the degradation in the maximum operational tempo of the network as the size of the network increases. The y-axis shows the maximum operational tempo in Hz and the x-axis represents the number of sensor nodes within the network.

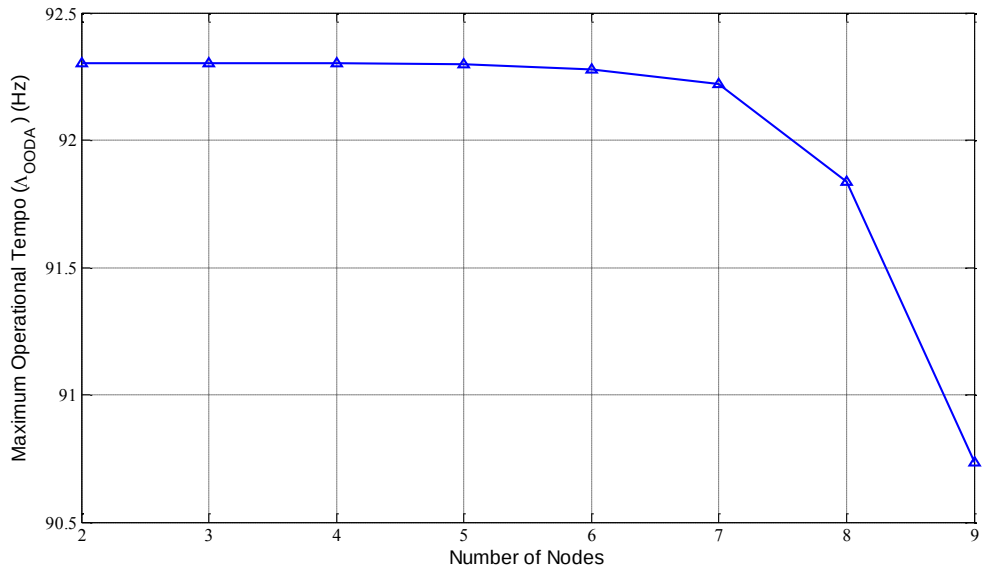

Figure 10. Maximum operational tempo degradation due to network expansion

The results in Figure 10 show that as the network increases in size, the rate in which the network can complete an OODA loop degrades. The maximum operational tempo will monotonically decrease if the number of nodes increases beyond nine as shown in Figure 10. Results for networks greater than nine nodes are not provided due to the amount of time required to complete the simulations. Although more simulation

results are not presented for networks greater than nine nodes the data from Figure 10 is fitted using a polynomial fit to predict the remainder of the degradation. Figure 11 is provided to show the polynomial fit prediction for the maximum operational tempo decline as the network size continues to increase to 35 nodes.

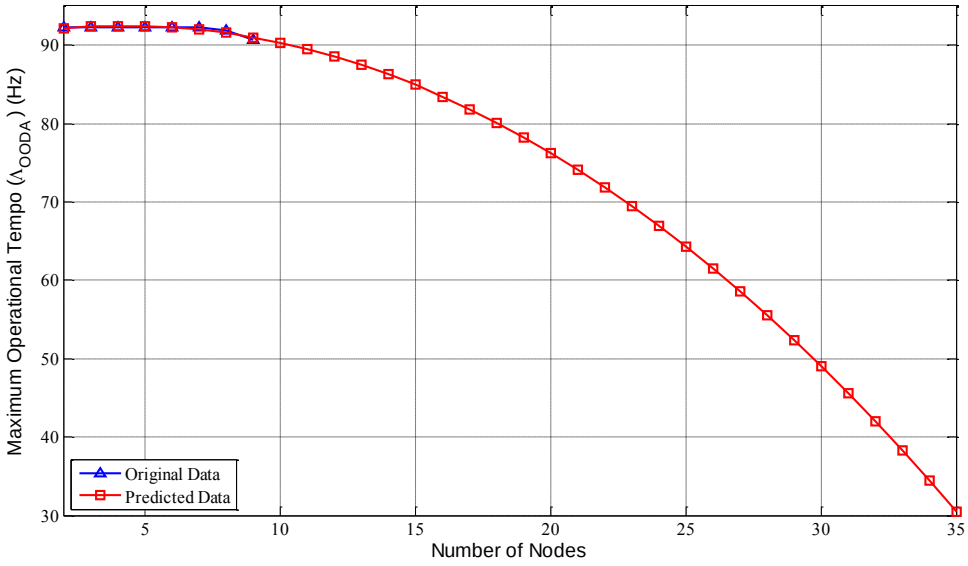

Figure 11. Maximum operational tempo prediction as network size increases

The prediction presented in Figure 11 shows the continuous decline of the maximum operational tempo as the network continues to increase in size from two to 35 nodes. Without the parallel processing capability this cannot be verified, but based on the results generated it is assumed that this trend will continue downward until Λ_{OODA} reaches zero. This means there will be a specific number of nodes a network will be able to sustain while still being able to make autonomous decisions. Once the network size causes Λ_{OODA} to reach zero, the network will no longer be capable of decision-making. This prediction is for a static configuration, but as the number of nodes is increased, the trend could potentially be reversed if node optimization can be performed.

C. DYNAMIC SCENARIO

The simulation results provided for the static simulation display an interesting observation in how network performance degrades as the network increases in size. The static scenario is basic; however, it highlights an important point which must be considered when designing a sensor networks layout prior to employment. With the static scenario in mind, this section utilizes LPISimNet(V)3 again to simulate the effects of a dynamic scenarios size. Although the degradation of the maximum operational tempo will continue as the network size increases, it can be slowed, and the additional degradation due to range can be offset by the proper placement of static nodes throughout the network. This section first describes the dynamic scenario in detail. Next, the simulation results are presented to include: node capability, characteristic tempo, and maximum operational tempo.

1. Scenario Setup

The simulations conducted in this section involve a dynamic scenario's size that increases from three to six nodes. The scenarios are meant to simulate a military situation having multiple aircraft, or unmanned aerial vehicles (UAVs) flying along specified routes, collecting information, while being controlled by air traffic control (ATC) stations. Due to the potential difficulties in communicating with these aircraft at great distances, repeaters, or communication relay stations, are displayed to extend the communication range between nodes. There are a total of four simulations presented, including a three-, four-, five-, and six-node network. Each network builds upon the previous network, with the inclusion of a single node for each simulation. The geometry of each network is provided next, along with the description of each node, and the communications parameters they employ.

a. Scenario Geometry

The three-node scenario serves as the baseline for the remaining networks. Figure 12 displays the scenario setup for the three-node simulation using LPISimNet(V)3. The three nodes include one UAV, one ATC station, and one repeater labeled UAV1, ATC1, and Repeater1, respectively. The blue circles represent the moving (dynamic) node,

while the blue triangles represent the stationary (static) nodes. The green arrows represent the communication links between nodes with the arrows reflecting the direction in which communication can travel. The black dashed line reflects the direction of movement of the dynamic node from the starting position (time index one) to the final position (time index five). The dimensions of the simulation are labeled on the grids in kilometers. The network is expanded to four nodes with the inclusion of a second UAV, labeled UAV2. Figure 13 shows the geometry of the four-node network. Again, the scenario is expanded to include a fifth node, another ATC station, labeled ATC2. Figure 14 is presented to show the geometry of the five-node network. Finally, the network increases in size with the inclusion of a final repeater, labeled Repeater2, for a total of six nodes. Figure 15 shows the final layout of the six-node network.

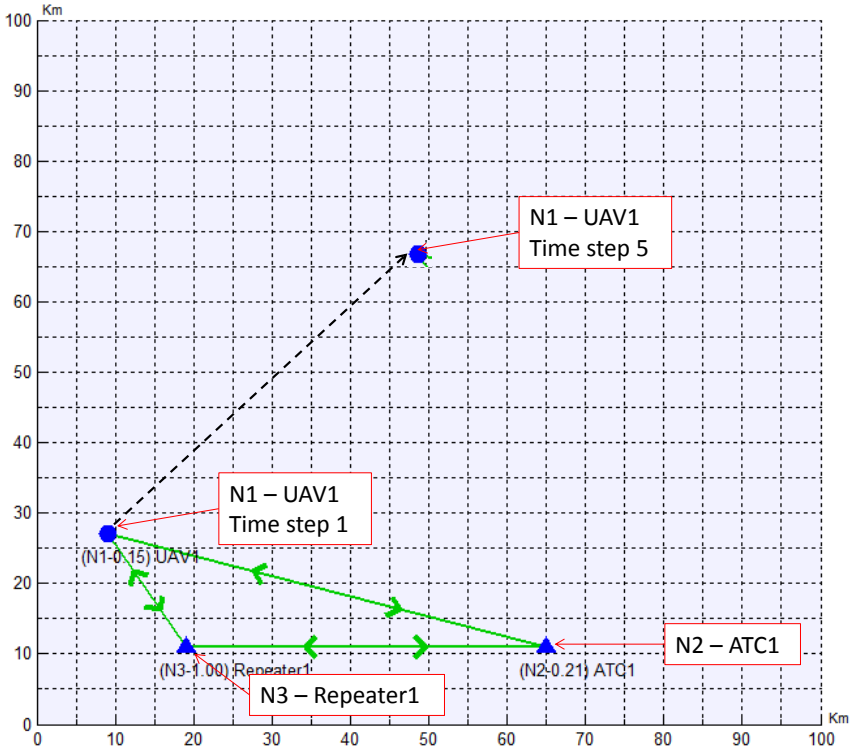

Figure 12. Simulation geometry for three-node dynamic network

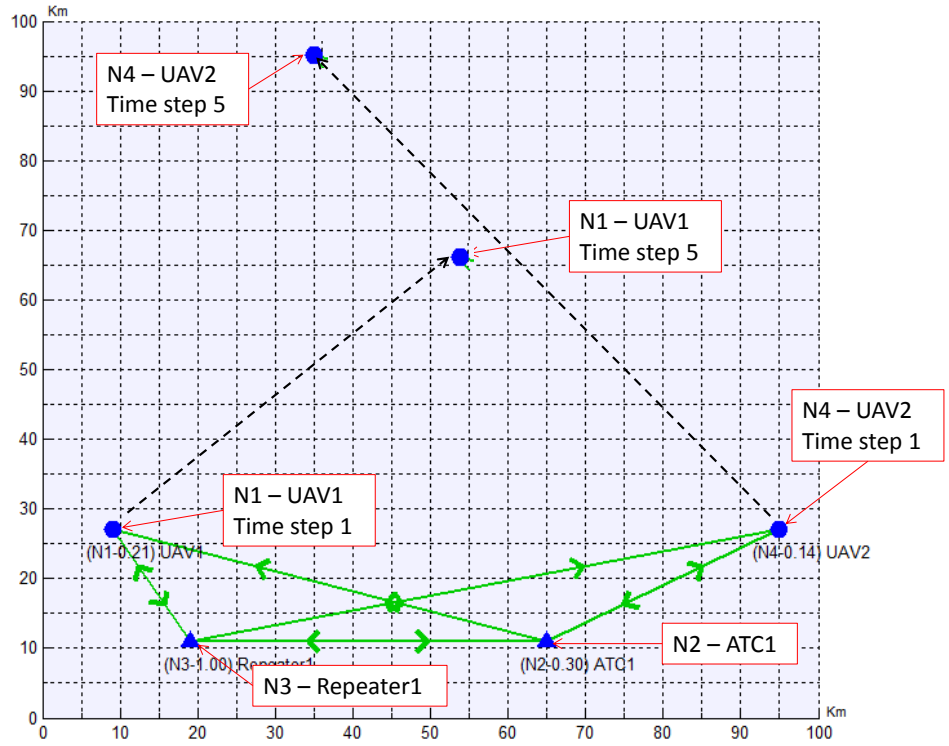

Figure 13. Simulation geometry for four-node dynamic network

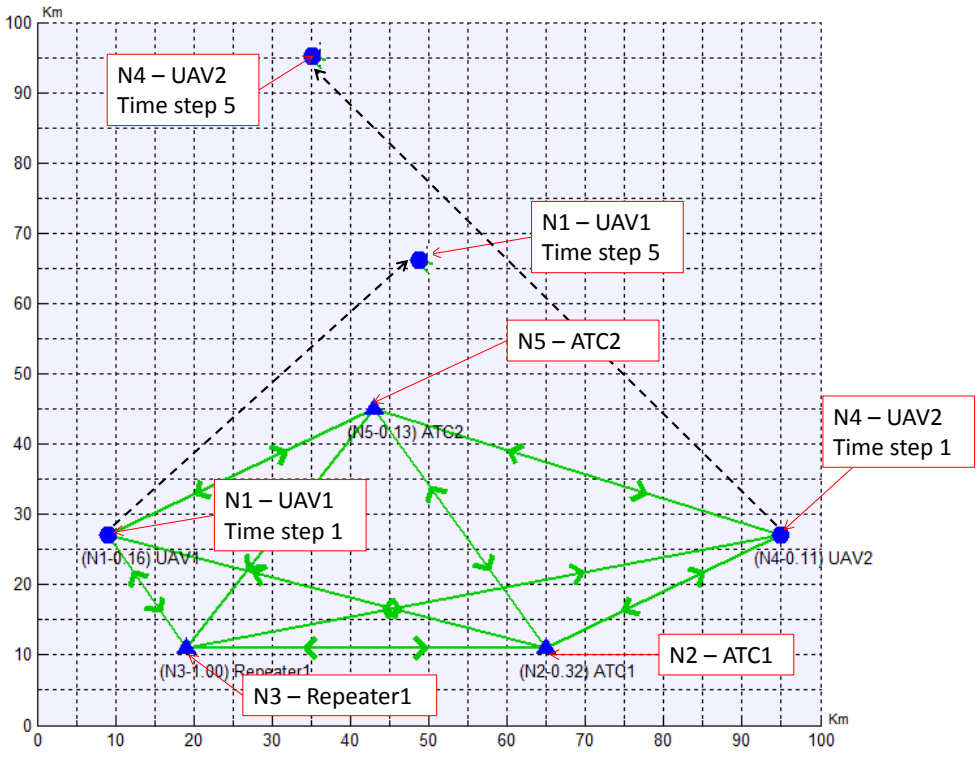

Figure 14. Simulation geometry for five-node dynamic network

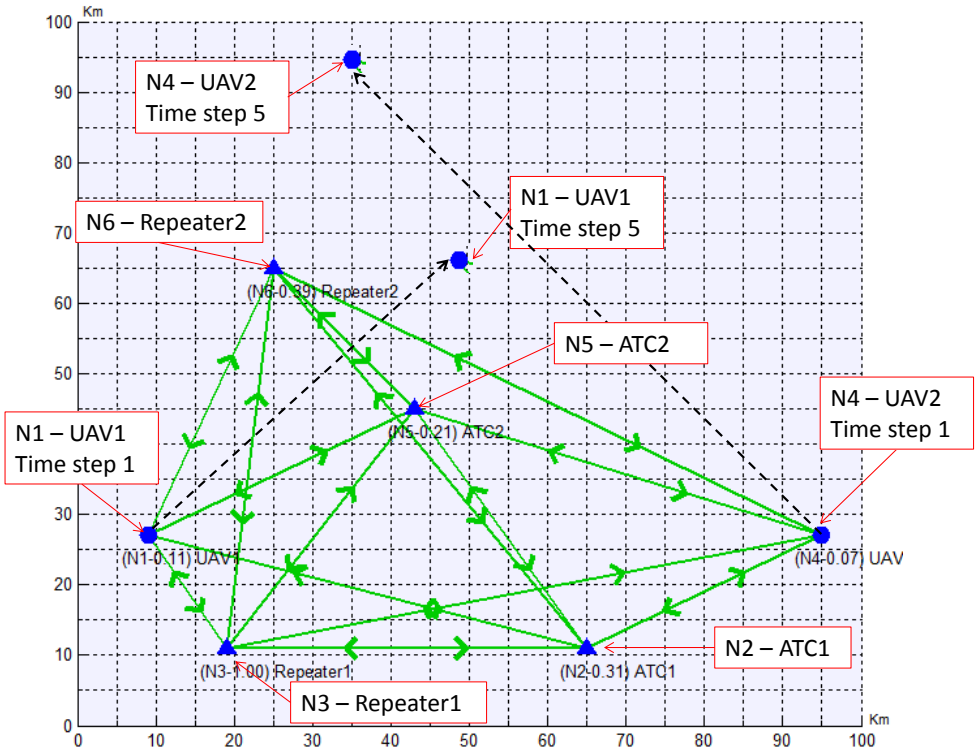

Figure 15. Simulation geometry for six-node dynamic network

b. Node 1 – UAV1

UAV1 represents one of the two dynamic nodes, which acts as a sensor to collect and disseminate imagery to one or both of the command and control (C2) stations (ATC1 and/or ATC2) and receive routing commands from the C2 stations. Due to the distance and possibility of obstacles interfering with line-of-sight communications this sensor imagery and routing commands may be relayed to and from the UAV through a repeater station.

c. Node 2 – ATC1

The ATC station reflects where human decision-makers reside, the C2 facility, relying on the information disseminated by the UAVs to generate intelligence or action. The ATC station includes a human-computer interface that incorporates semi-autonomous decision-making, with the capability to conduct fully autonomous operations if needed. Although the information collection is a major function of this C2 facility, it is also concerned with the routing and safety of flight of the UAV, especially when

additional aircraft are added to the scenario. The ATC station has radars to help track the location of aircraft as well as a robust communications infrastructure, which enables them to communicate with multiple aircraft simultaneously.

d. Node 3 – Repeater1

Repeater1 represents a communications repeater station that forwards information between nodes that must communicate with one another. The repeater is not meant to make autonomous decisions, but only assist in the collection and retransmission of information between the ATC stations and the UAVs.

e. Node 4 – UAV2

UAV2 represents the second dynamic node added to the network. It has the same capabilities as UAV1. However, with the inclusion of a second aircraft within the airspace, the ATC stations must now be concerned with collision avoidance.

f. Node 5 – ATC2

The second ATC station is added to make the total network size five nodes. ATC2 is another static C2 node which is also where information collection and decision-making occurs. The same semi-autonomous/fully autonomous decision-making capability of ATC1 resides at ATC2 as well. Due to the distributed nature of many areas of operation, the addition of a second ATC is realistic. This allows for passage of control of the UAVs routing as they transit from one area to another. This is similar to civilian aviation, as they are required to switch between control towers as they transit across different regions.

g. Node 6 – Repeater2

Repeater2 represents the last static node added to the network, which brings the total to six nodes for the final scenario. It has the same responsibilities and capabilities as Repeater1. No autonomous decisions are being made by the repeater. It is solely responsible for collection and retransmission of information to and from the UAVs and ATC stations.

h. Node Parameters

The physical capabilities of the nodes described are not the important components of the analysis to follow. However, they provide a general picture for what the scenario represents. There are numerous parameters used for each node. Unlike the static scenario, not every node has the same communication parameters. Table 6 shows the detailed transmit and receive parameters used in LPISimNet(V)3 to conduct the simulation for the six nodes used in the four simulations.

Table 6. Communications parameters for six nodes

Node Index	**1**	**2**	**3**	**4**	**5**	**6**
Name	N1-UAV1	N2-ATC1	N3-Repeater1	N4-UAV2	N5-ATC2	N6-Repeater2
Type	Friendly	Friendly	Friendly	Friendly	Friendly	Friendly
Position	(9,27)	(65,11)	(19,11)	(95,27)	(43,45)	(25,65)
Velocity (km/time index)	(10,10)	(0,0)	(0,0)	(-15,17)	(0,0)	(0,0)
Transmitted Power (W)	10	10	10	20	5	5
Transmitted Antenna Gain (dB)	10	20	20	10	18	20
Transmitted Frequency (GHz)	12	14	14	12	14	14
Packet Arrival Rate (packets/s)	3000	3000	3000	3000	3000	3000
Packet Length (bits)	4608	4608	4608	4608	4608	4608
Frame Length (ms)	5	5	5	5	5	5
Packet Error Rate	10^{-4}	10^{-4}	10^{-4}	10^{-4}	10^{-4}	10^{-4}
Modulation Scheme	M-QAM	M-PSK	B-PSK	M-QAM	M-PSK	B-PSK
Maximum Data Rate Allowed (Mbps)	36	24	6	36	24	6
Signal Element Combinations	64	16	2	64	16	2
Raised Cosine Filter Factor	0.5	0.5	0.5	0.5	0.5	0.5
Probability of Bit Error - Rx	10^{-3}	10^{-3}	10^{-3}	10^{-3}	10^{-3}	10^{-3}
Receiver Bandwidth (MHz)	10	10	10	10	10	10
Antenna Gain (dB)	10	20	15	10	20	15
Noise Factor - Rx	3	3	3	3	3	3
Implementation Loss	3	6	1	1	10	1

The parameters in Table 6 are for all nodes used in the four separate simulations. The three-node network only includes nodes one through three. The four-node network includes nodes one through four. This same pattern continues for the five- and six-node networks.

2. Results

The overall metrics used to analyze the performance of the network as the size increases from three to six nodes include; node capability value K_μ, connectivity measure C_M, network reach I_R, characteristic tempo λ_T, and maximum operational tempo Λ_{OODA}. The results from LPISimNet(V)3 for the three-, four-, five-, and six-node simulations are provided in Table 7 for time index, one, three, and five.

Table 7. LPISimNet(V)3 results for three time indexes of four networks

3-Node Network				
Time Index		1	3	5
Metrics		Value	Value	Value
K_μ	N1 - UAV1	0.15	0.05	0.03
	N2 - ATC1	0.21	0.21	0.21
	N3 - Repeater1	1.00	0.60	0.51
C_M		3.2137	2.0362	1.7280
I_R		0.3571	0.2262	0.1920
R_Q (MHz)		3.84098424	3.89017782	3.74649052
λ_T (MHz)		1.37153666	0.88012725	0.71932592
Λ_{OODA} (Hz)		92.2891	92.2787	92.2722
4-Node Network				
Time Index		1	3	5
Metrics		Value	Value	Value
K_μ	N1 - UAV1	0.21	0.07	0.04
	N2 - ATC1	0.30	0.25	0.21
	N3 - Repeater1	1.00	0.63	0.52
	N4 - UAV2	0.14	0.08	0.03
C_M		6.9126	4.2131	3.0909
I_R		0.2160	0.1317	0.0966
R_Q (MHz)		3.01587340	2.93183950	2.52709500
λ_T (MHz)		0.65148436	0.38599991	0.24409458
Λ_{OODA} (Hz)		92.2685	92.2415	92.2031

5-Node Network				
Time Index		1	3	5
Metrics		Value	Value	Value
K_μ	N1 - UAV1	0.17	0.15	0.06
	N2 - ATC1	0.32	0.28	0.25
	N3 - Repeater1	1.00	0.69	0.60
	N4 - UAV2	0.12	0.11	0.04
	N5 - ATC2	0.13	0.25	0.16
C_M		16.1765	16.4059	9.4914
I_R		0.1348	0.1367	0.0791
R_Q (MHz)		3.10996550	3.60923050	3.09054776
λ_T (MHz)		0.41923618	0.49343804	0.24444632
Λ_{OODA} (Hz)		92.2468	92.2559	92.2032
6-Node Network				
Time Index		1	3	5
Metrics		Value	Value	Value
K_μ	N1 - UAV1	0.15	0.23	0.11
	N2 - ATC1	0.31	0.28	0.25
	N3 - Repeater1	1.00	0.76	0.69
	N4 - UAV2	0.10	0.13	0.11
	N5 - ATC2	0.21	0.31	0.23
	N6-Repeater2	0.39	0.57	0.54
C_M		61.4162	80.5930	58.7815
I_R		0.1150	0.1509	0.1101
R_Q (MHz)		3.67283269	4.04920392	3.70756631
λ_T (MHz)		0.42241808	0.61111923	0.40812010
Λ_{OODA} (Hz)		92.2472	92.2659	92.2451

Table 7 shows a snapshot of the network metrics that are analyzed in the following sections. LPISimNet(V)2 was not designed to analyze multiple networks simultaneously. Therefore, LPISimNet(V)3 is used, without the network comparison file, to generate individual network results and combine them as a means to provide a visual

depiction of the effects of increasing the network size on the node capability, characteristic tempo and ultimately the maximum operational tempo.

a. Node Capability Analysis

The node capability of an individual node is dictated by the link properties between it and its directly connected nodes [12]. Node capability analysis for an individual network was provided in [12]; however, the effect of increasing the networks size is not considered. As the network size increases from three to six nodes, the number of links between nodes increases, which may cause variation in the node capability values. Additionally, similar to the analysis conducted in [12], due to the motion of the dynamic nodes in each scenario, there is an expected variation in the node capabilities as the distances between nodes varies, which ultimately causes the SNR between nodes to change.

The nodes analyzed in this section are the three nodes from the original scenario: UAV1, ATC1, and Repeater1. These nodes were selected because they are common throughout each scenario. Figure 16 also shows the node capability values for UAV1 over the five time indexes for the three-, four-, five-, and six-node network scenarios. The results in Table 7 indicate that UAV1 is the least capable node (of the original three) based on its node capability value. Figure 16 shows the variation in node capability for UAV1 not only as the node moves throughout the scenario, but also as the number of connections increases. As the network increases from three to six nodes, the static state node capability, at time index one, varies only slightly from 0.15 to 0.21. This shows the node capability value of UAV1 has little dependence on the network size. Although the network size has a limited impact on the node capability of UAV1, the distance between nodes (or the motion of the nodes) has a substantial impact.

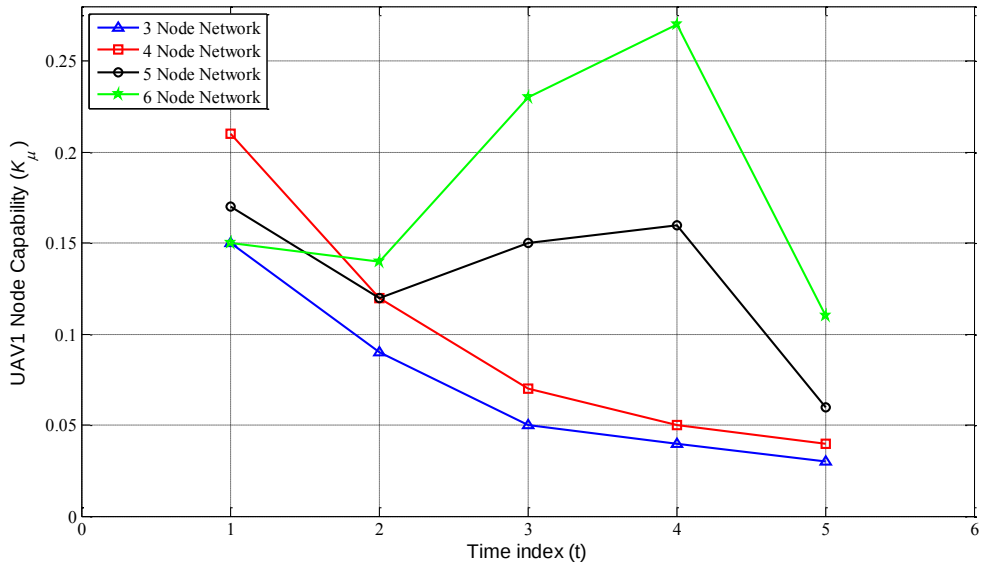

Figure 16. Node capability values for UAV1 over five time indexes

Figure 16 shows that for the three- and four-node scenarios, there is a constant decline in node capability. This is due to the SNR decrease between UAV1 and Repeater1 and ATC1. The increase in node capability for the five- and six-node networks is due to the forming of a "bracket" around UAV1 with the additional static nodes, ATC2 and Repeater2.

The term bracket is used in Marine Corps Artillery when an observer is attempting to adjust rounds onto a target. The bracket is formed when one round lands in front of the target and another round lands behind the target along the observer-target line. In terms of a sensor network with dynamic nodes, the node's path would represent the targets and the bracket would be formed by static nodes. Figure 17 displays the bracket concept for a general sensor network with dynamic nodes. The triangles represent static nodes, the circles represent dynamic nodes, the dynamic nodes path is reflected by the dashed line, and it is assumed that each node is fully connected.

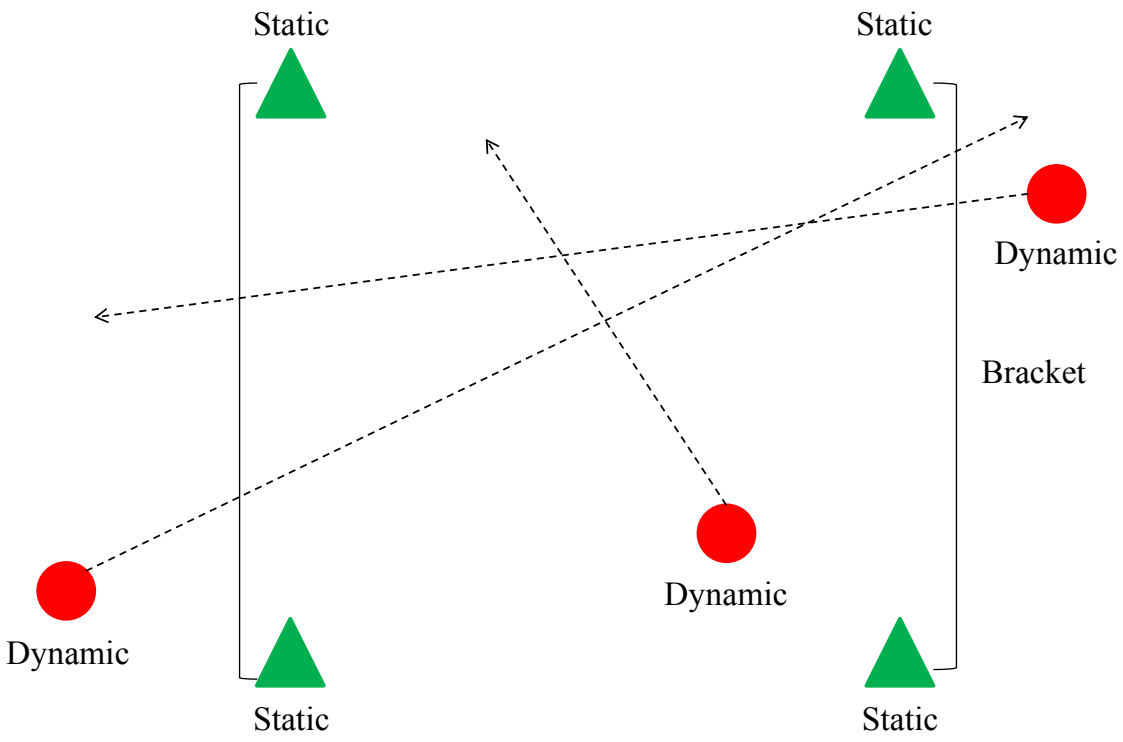

Figure 17. Example of bracket concept

The next node analyzed was ATC1. Figure 18 displays the node capability values of ATC1 over the five time indexes for each scenario. The node capability value for ATC1 shows a variation in the node capability value as the number of direct links increases. Figure 18 shows that at time index one there is an increase in the capability value as the network gets larger. The outlier point is the difference between the five- and six-node networks, where the node capability value actually drops with the addition of the sixth node. Additionally, there is also a decline in the capability value as the dynamic nodes in the scenario move away from ATC1. This is an expected result; the static node's link between the two dynamic nodes is being degraded as range between the nodes increases. This causes the SNR to decrease with range, which ultimately reduces the data throughput, causing the node capability value to decline.

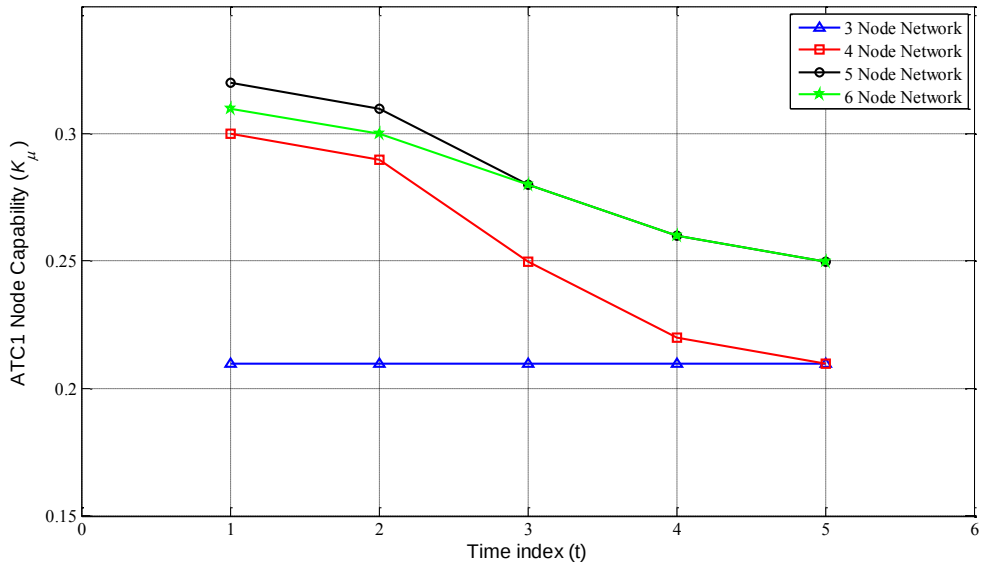

Figure 18. Node capability values for ATC1 over five time indexes

The final node capability value analyzed is for the static node, Repeater1. Figure 19 displays the node capability values for Repeater1 as the network increases in size from three to six nodes, as well as the decline in node capability over the five time indexes for each scenario due to range. As the number of directly connected nodes increases from two to five, the node capability of Repeater1 stays the same at time index one. This is because Repeater1 was the most capable node in the network from the beginning. Due to $0 \leq K_\mu \leq 1$ being a requirement, the node capability value of Repeater1 is not permitted to exceed one. Figure 18 shows that there is an increase in the node capability value as a result of the directly connecting links. As the scenario moves from static to dynamic from time index two to five, the node capability value is greatest for the six-node network. Additionally, there is a noticeable decline in Repeater1's capability value as the dynamic nodes (UAV1 and UAV2) move away. This again is an expected result due to the SNR decreasing as a function of range, yielding a declining data throughput, and finally a degrading capability value.

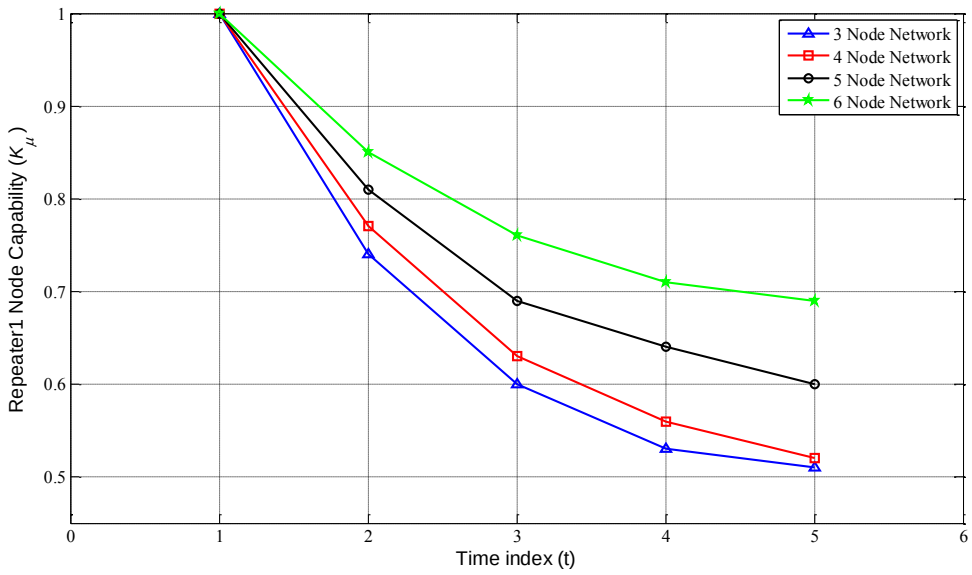

Figure 19. Node capability values for Repeater1 over five time indexes

This section highlighted the effects on the node capability value of three nodes as the number of directly connected nodes increases and the distance between static and dynamic nodes change. The next section shows the effects of network size on the characteristic tempo of the network.

b. Characteristic Tempo Analysis

The characteristic tempo λ_T of a network represents the rate at which information can be shared, and is the product of the network reach I_R and network richness R_Q [6]. Network reach I_R is dictated by the connectivity measure C_M and the reference connectivity measure C_M^R. The reference connectivity measure C_M^R is ultimately a function of the network size. As the size of the network increases, C_M^R increases. Equation (4) is presented again to show this relationship and Table 8 shows a summary of C_M^R values for networks including three to 15 nodes.

$$I_R = \frac{C_M}{C_M^R}$$

Table 8. Reference connectivity measure for 3-15 node networks, from [11]

Number of Nodes	C_M^R
3	9
4	32
5	120
6	534
7	2905
8	18976
9	144648
10	1256730
11	12232913
12	131714208
13	1553256848
14	19901596974
15	275225101905

As shown in Table 8, the reference connectivity measure increases from nine to 534 as the network size increases from three to six nodes. This causes an expected decline in the network reach as the reference connectivity measure is in the denominator. Figure 20 provides the I_R values for each network configuration over five time indexes.

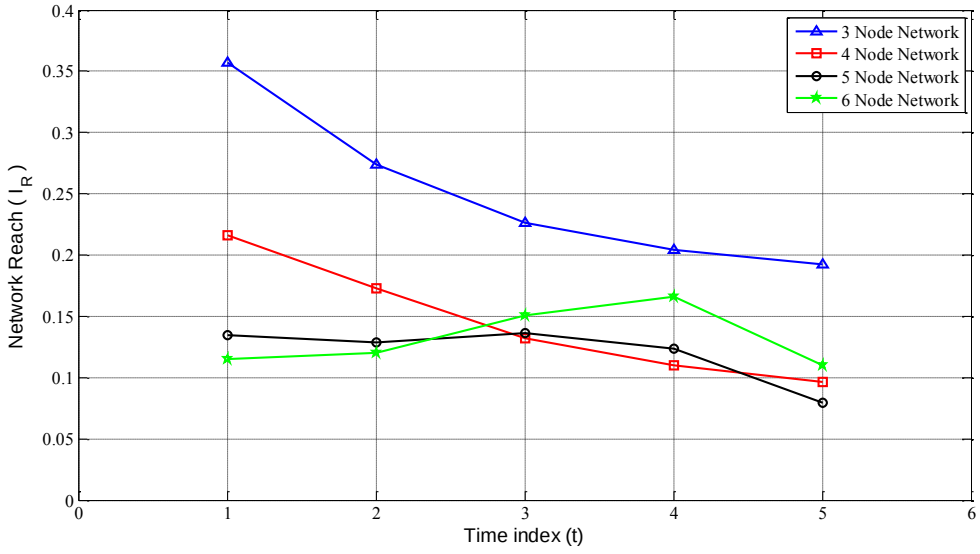

Figure 20. Values of network reach over five time indexes

At the static state (time index one), there is a noticeable decline in the network reach, which is purely a function of the network size, resulting in the increase from the reference connectivity measure. This degradation can be offset by increasing the connectivity measure, which does not normally increase at the same rate as C_M^R. A major component of the connectivity measure is the length of the routes between nodes (or the distance between nodes) [6]. By creating a shorter path for information to flow between nodes, the connectivity measure should increase. Figure 20 displays that with the proper placement of the fifth and sixth node, the network reach begins to increase as the range between the dynamic and new static nodes decreases. This ultimately assists in offsetting the degradation due to the reference connectivity measure.

With the degradation due to the reference connectivity measure being offset by node placement the next metric to analyze is the characteristic tempo λ_T. It is expected that λ_T follow the same pattern as I_R due to the mathematical relationship. Equation (7) is provided again to show the relationship between λ_T and I_R.

$$\lambda_T = I_R R_Q \quad \text{Hz}$$

With I_R decreasing as a function of the network size at the static state, λ_T does as well. Figure 21 displays the values of the characteristic tempo versus the number of nodes in the network at time index one. As expected, the characteristic tempo declines as a function of network size. Additionally, the rate of decline due to the network size is slowed with the addition of the sixth node in a geometrically sound location to enhance the information exchange capability.

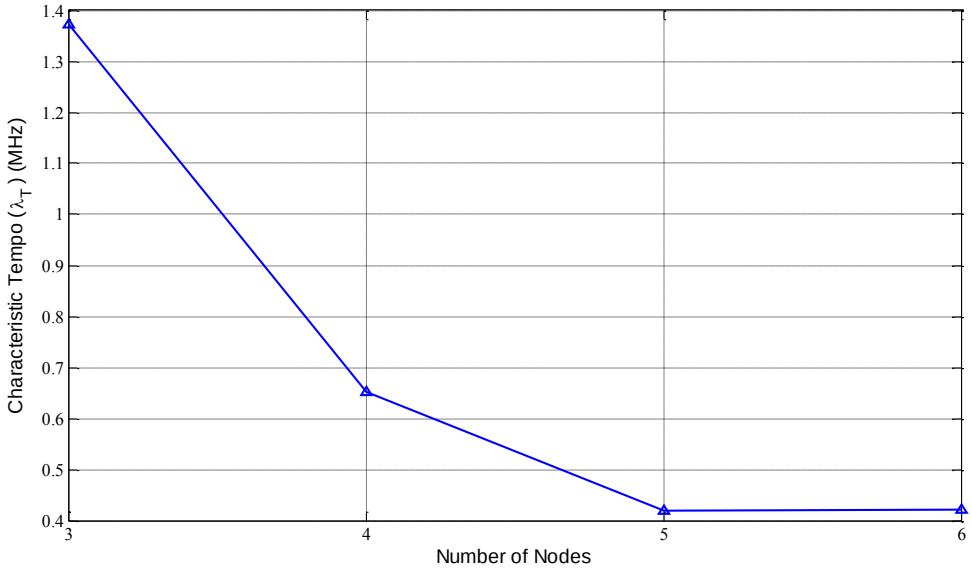

Figure 21. Characteristic tempo vs. number of nodes at time index one

Figure 22 is provided to show the values of the characteristic tempo for each network configuration over five time indexes. The comparison of Figure 20 with Figure 22 shows that λ_T follows the exact same pattern as I_R. As the number of nodes increases, there is a decline in rate at which the network can share and exchange information. Also, as the range between the static and dynamic nodes increase, there is a continued degradation in the characteristic tempo. However, by "bracketing" the dynamic nodes, with the fifth and sixth nodes, the decline due to range is offset, causing λ_T to increase to values at or above the values of the four-node network.

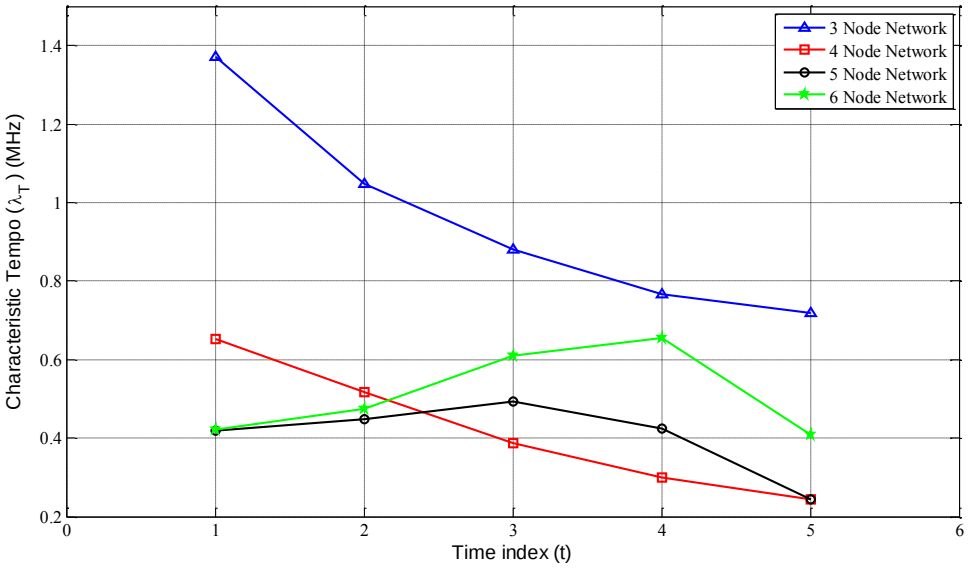

Figure 22. Values of characteristic tempo over five time indexes

c. Maximum Operational Tempo Analysis

For a military force, the ability to adapt to environmental changes or enemy action often dictates success or failure. This is often equated to the rate at which a force can complete an OODA loop. The capability of a military force's network to complete an OODA loop is defined as the maximum operational tempo [6]. The maximum operational tempo, equation (8), is repeated below for the convenience of the reader.

$$\Lambda_{OODA} \le \frac{1}{\left(\Delta t_1 + \Delta t_2 + \Delta t_3 + \Delta t_4\right)} \le \frac{\lambda_{C2}}{1 + \left(\frac{1}{\lambda_d} + \frac{1}{\lambda_f}\right)\lambda_{C2} + \frac{3\lambda_{C2}}{\lambda_T}} \quad \text{Hz}$$

As shown by Figure 5, the action tempo which generates the most change in the maximum operational tempo is the command and control tempo λ_{C2}. The model assumes that all action tempos, λ_{C2}, λ_d, and λ_f are constant values through all time indexes simulated. With this being the case, the only factor which dictates change in the maximum operational tempo throughout a given scenario is the characteristic tempo.

With the position of λ_T in (8), it is expected that Λ_{OODA} follow the same pattern as λ_T, or be affected in the same way.

Much like the time index one results for λ_T the static state results for Λ_{OODA} show that there is a decline in the maximum operational tempo of the network as the number of nodes increases, and a slight improvement with the proper placement of the sixth node. Figure 23 displays the values of the maximum operational tempo versus the number of nodes in the network at time index one.

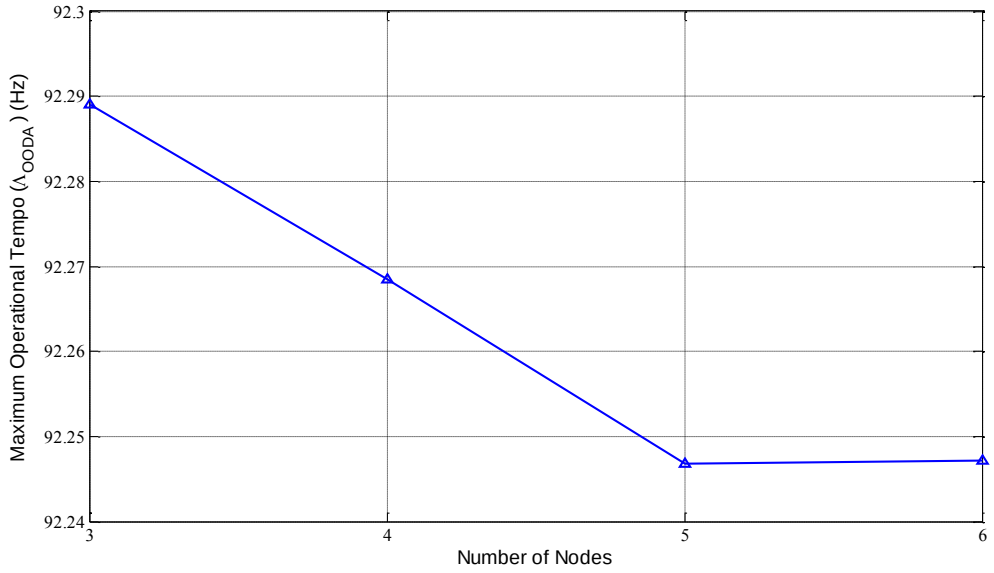

Figure 23. Maximum operational tempo vs. number of nodes at time index one

Although the static states degradation cannot be fully offset with the addition of the fifth and sixth nodes without node optimization, the degradation due to range can, just as with the characteristic tempo. Figure 24 shows the values of Λ_{OODA} over five time indexes for each network topology. When the network moves from static to dynamic, from time index two through five, there is a continued degradation in the maximum operational tempo, for the three- and four-node networks, as the range between the dynamic nodes (UAV1 and UAV2) increases away from the static nodes (ATC1 and Repeater1). The rate at which the network can complete and OODA loop increases from

time index two to four for the five- and six-node networks, which is due to the range between UAV1 and UAV2 decreasing between ATC2 and Repeater2. Another decline occurs between time indexes four and five, which is when the dynamic nodes are again moving away from ATC2 and Repeater2. The increase shown for the five- and six-node networks means the networks information exchange and decision-making capability is increasing due to the improvement of C_M as a result of the bracket formed by the static nodes of the network.

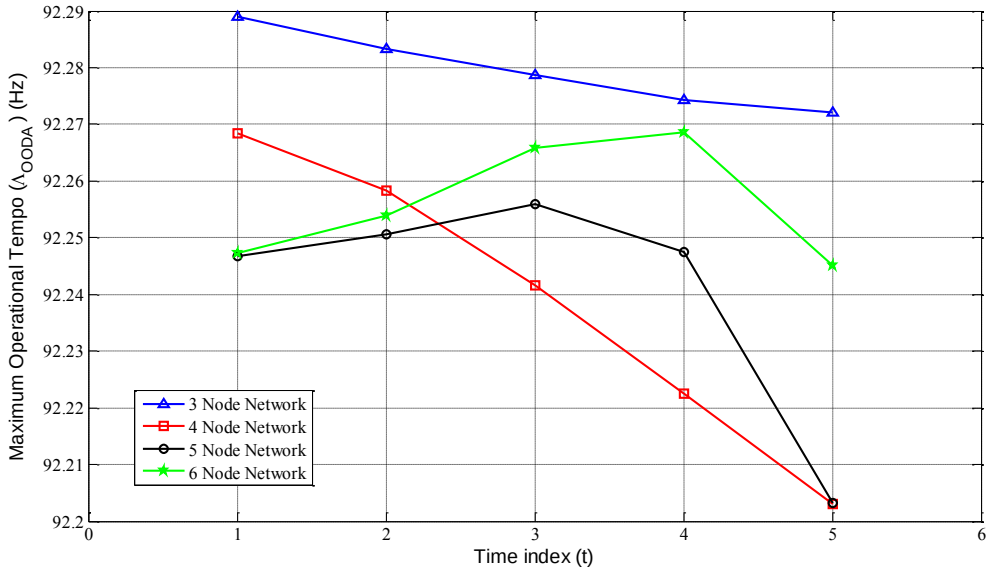

Figure 24. Values of maximum operational tempo over five time indexes

The maximum operational tempo is an important network capability metric to be considered when planning network operations. The maximum operational tempo Λ_{OODA} can be used as a network comparison tool to determine which network topology is the most efficient to use prior to employment. Additionally, it can be used to measure how effective a friendly network is in comparison to a known enemy capability. The fact that Λ_{OODA} declines as the network size increases is an important point to highlight. Just because a large number of sensors are employed does not necessarily mean the

knowledge generated by the network of sensors will be more efficient or effective than the knowledge generated by a network with a smaller number.

D. CONCLUSION

Although the scenarios in this chapter are basic, their results highlight the significance of this thesis investigation. As the size of a sensor or communications network increases, the rate at which information can be turned into knowledge decreases. This provides a decision-maker with a bit of a dilemma about how to structure their network. Is the amount of information that can be collected more valuable than the rate at which that information can generate knowledge?

Also, in a scenario with moving sensors, a method for offsetting the degradation of the characteristic tempo and maximum operational tempo was provided. By bracketing the dynamic nodes in the network, λ_T and Λ_{OODA} showed improvement as UAV1 and UAV2 moved along their respective routes. The dynamic scenario could also be used to show the best layout for a static sensor network. Time index four, for the six-node network, displayed the highest rate of completing an OODA loop. With that being the case, the best geometric makeup of the network would be when the nodes are placed in the locations specific to time index four. This also shows that by simulating a static network with dynamic nodes can assist in determining the most efficient static network to employ.

The next chapter is devoted to highlighting additional practical considerations. The robustness of a network can be tested by showing the effects of electronic attack on the network and how it affects the characteristic and maximum operational tempos. Additionally, the possibility of varying the C2 tempo of the network is explored. Also, the relationship between data throughput and SNR is discussed. Finally, a network comparison tool is presented to provide a decision-maker with a method to determine the best network topology to deploy.

V. PRACTICAL CONSIDERATIONS

A. INTRODUCTION

Many considerations for network operations are presented in previous studies. The effect of electronic attack in [11] is shown prior to the inclusion of the adaptive node capability metric. The interaction of action tempos according to different Sheridan Levels is displayed in [12], but does not consider the potential of the C2 tempo varying as a situation changes. The relationship between data throughput and SNR is described in [12] also; however, the full relationship is not shown due to the assumption of three node parameters, packet arrival rate (PAR), packet length, and frame length, being the same. In addition to these considerations, the modeling tool, LPISimNet(V)3 has the potential for added utility for network comparison, which would allow a decision-maker to compare two network simulations in order to determine the best network topology to deploy.

This chapter focuses on these specific considerations. The five-node network is used to display the effects of electronic attack on the characteristic and maximum operational tempos of the network using LPISimNet(V)3. Second, maximum operational tempo results are displayed considering that the C2 tempo of the network could potentially vary as the scenario unfolds. Next, to answer the question of SNR dependency of data throughput, the five node network is used to produce results of link based SNR and data throughput for each node. Finally, a new network comparison tool added to LPISimNet(V)3 is described along with example results to assist a commander in determining the best network solution to employ.

B. NETWORK ASSURANCE IN THE PRESENCE OF ELECTRONIC ATTACK

The robustness of any system cannot be fully tested until it has to deal with adversity. The addition of new technologies to the battlefield opens new vulnerabilities to be exploited. When a force is employing any variety of wireless sensor networks, the potential for enemy interference is present. Prior to employment of any network, it is

important to consider the potential ramifications of network degradation, or test the network assurance, or robustness, of the network in the presence of denial of service attacks. With the characteristic and maximum operational tempos being key metrics to determine overall network performance the effects of electronic attack on these metrics are presented.

The five-node dynamic network is used to display the effects of link suppression on λ_T and Λ_{OODA}. The five-node network results in Figure 14 provide the baseline starting point for the network, where no electronic attack is present. By removing the sensor network receivers one at a time the effects of electronic attack can be quantified. All links removed are connected to UAV2. The first link removed is between UAV2 and ATC2 (1 link suppressed). Following that, Repeater1's receive link from UAV2 is removed (1.5 links suppressed). Next, UAV2s receive link from Repeater1 is removed (2 links suppressed). Finally, the UAV2s receive link from ATC1 is removed (2.5 links suppressed). Figure 25 displays the final layout of the five node network after 2.5 links are eliminated due to electronic attack. Comparing Figure 14 and Figure 25 provides the start and end points of the network suppression.

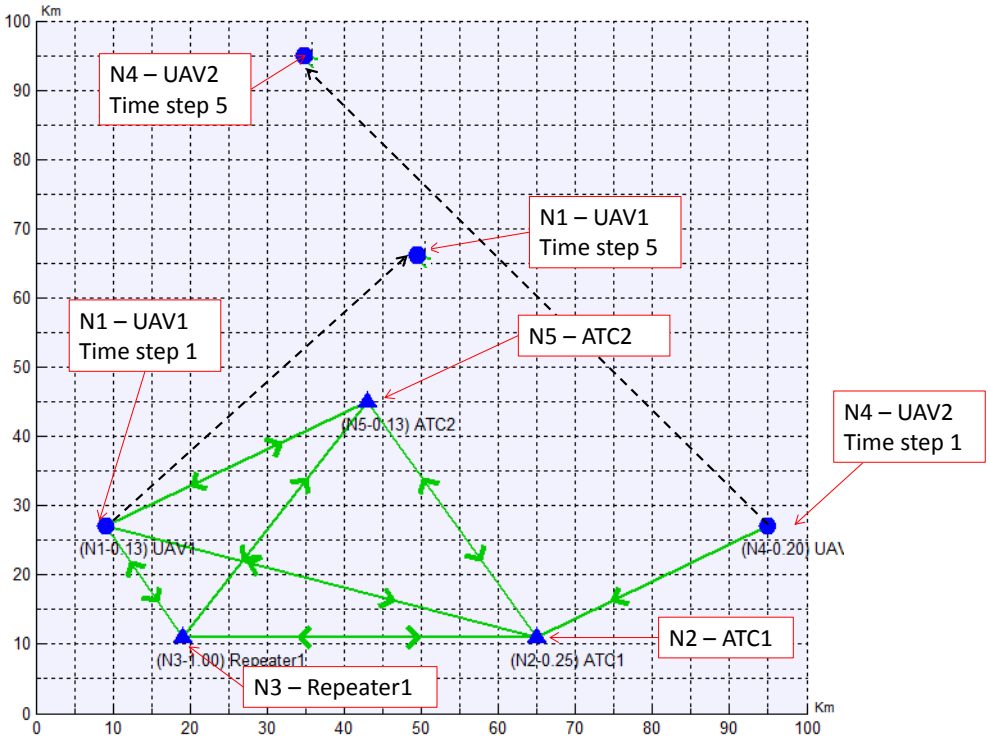

Figure 25. Five-node network with 2.5 links suppressed

If all links connected to UAV2 are actually removed from the network there would be an increase in λ_T and Λ_{OODA}. This would cause the network to appear to be performing more efficiently, when in fact the network is actually losing sensing capability with the removal of one of its primary collection assets. With UAV2 maintaining a portion of its communication capability, the effects of network suppression can actually be displayed. Figure 26 shows the effects of link suppression on λ_T over the five time indexes of the dynamic scenario. The most important factor displayed in Figure 26 is that as more links are removed from the network, the rate at which information can be shared declines. This is similar to the result displayed in [11], and shows that the inclusion of the adaptive node capability value does not change the result. These results also show that the network actually has a fairly robust structure. Even though there is a decline in the information sharing capability of the network, it is still functional even with multiple links being removed.

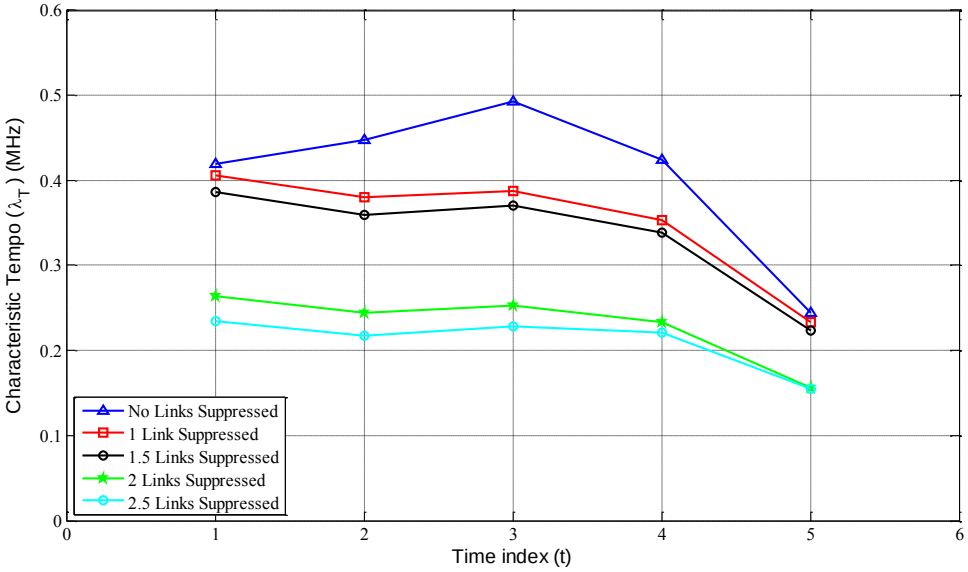

Figure 26. Values of characteristic tempo as links are suppressed

The maximum operational tempo Λ_{OODA} follows the same pattern as λ_T. This pattern holds true during electronic attack as well. Figure 27 shows the values of the maximum operational tempo as links are suppressed over the five time indexes in the dynamic scenario. Although the scales are different, Λ_{OODA} degrades, in the same manner as λ_T, as each link is removed from the network. This again is similar to the results presented in [11]. The results for Λ_{OODA} also show that the network's ability to complete the OODA loop may be degrading, but the network is still functional for the decision-maker.

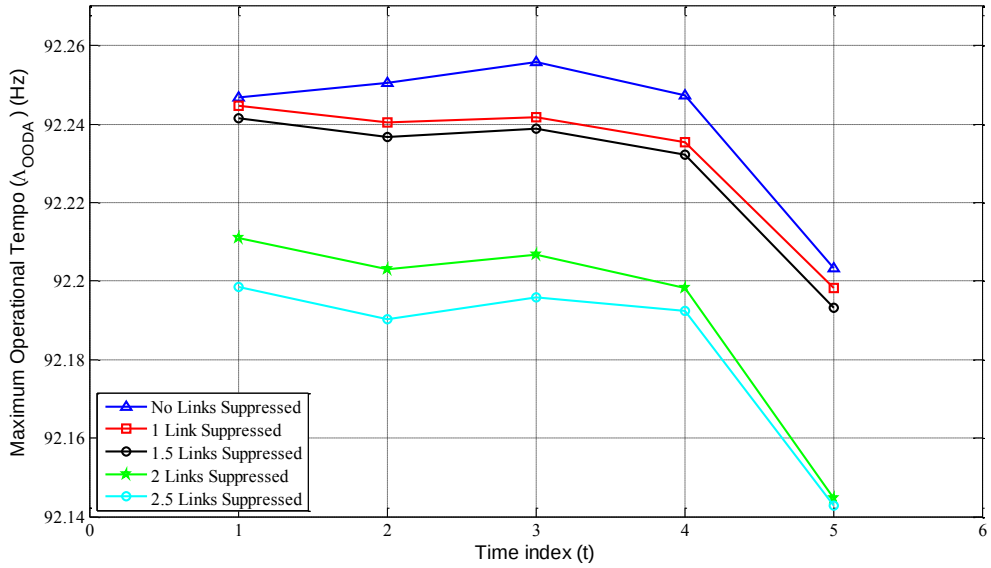

Figure 27. Values of maximum operational tempo as links are suppressed

The results show that as links are removed from the network, the rate at which information can be shared, and the rate at which the network can complete the OODA loop declines. These results validate those presented in [11], even after the inclusion of the adaptive node capability value.

C. VARYING DECISION-MAKING TEMPO

The second assumption present in [6] states that "for every C2 structure and the associated doctrine and degree of training and professional mastery, there is a characteristic decision-making speed, λ_{C2}." This assumption was adapted to the model in [11] and carried forward by [12]. It is shown in Figure 5, that varying λ_{C2} causes the greatest change to Λ_{OODA}. These models assume that λ_{C2} is a top level property, which does not change from the beginning of a situation, until it culminates. This section provides results using a different point of view; the characteristic decision-making speed could actually change as different situations unfold.

The decision-making speed of an autonomous network is tied to the Sheridan Level assigned. The Sheridan Levels of Authority describe the interaction that human

decision makers have with their respective autonomous systems [2]. With an autonomous decision-making network, the higher the Sheridan Level, the more decisions are being made without human interaction, and conversely, the lower the Sheridan Level, more decisions are being made with human input. Table 9 displays the Sheridan Levels of Authority with associated computer and human tasks.

Table 9. Sheridan Levels of Authority, from [2]

Level	Computer Task	Human Task
1	No assistance	Does all
2	Suggests alternative	Chooses
3	Selects way to do task	Schedules response
4	Selects and executes	Must approve
5	Executes unless vetoed	Has limited veto time
6	Executes immediately	Informed upon execution
7	Executes immediately	Informed if asked
8	Executes immediately	Ignored by computer

It is hard to quantify exactly how the human computer interaction will transpire as different situations come to light. It is easy to assign an initial level for a network after initial planning is conducted. However, due to environmental factors a decision-maker could choose to want more control over the process. On the other hand, the level of trust in the autonomous decision-making process could drive the operator to want less control, which would allow for the computer to conduct actions with minimal or no human input.

As an example, the five-node network is used. Figure 14 shows UAV1 and UAV2 on a path that appears to cross. The ATC stations are responsible for ensuring that the aircraft do not collide, which could either be done by time, lateral or altitude de-confliction. A human operator residing at either of the ATC stations may not trust the autonomous system to make these routing decisions properly and therefore take control of the situation. Based on the Sheridan Levels, this actually would reduce λ_{C2}, which would cause Λ_{OODA} to slow down. On the other end of the spectrum, the human operator may have full trust in the capabilities of the computer to make the routing decision,

therefore taking themselves out of the decision-making process entirely. This would cause the Sheridan Level to increase, ultimately leading to an increase in the maximum operational tempo. LPISimNet(V)3 allows for λ_{C2} to range from 100 Hz to 900 Hz. For the purposes of this section it is assumed that 100 Hz is Sheridan Level one and 800 Hz is Sheridan Level eight. Figure 28 is provided to show the effects of increasing and decreasing λ_{C2} on Λ_{OODA} for the five-node network over the five time indexes of the scenario. The blue line represents the standard medium action tempos employed by the original five node network. The red line shows the increase in Λ_{OODA} due to an increase in λ_{C2} from 100 Hz to 500 Hz. The black line displays the decrease in Λ_{OODA} due to a decrease in λ_{C2} from 500 Hz to 100 Hz.

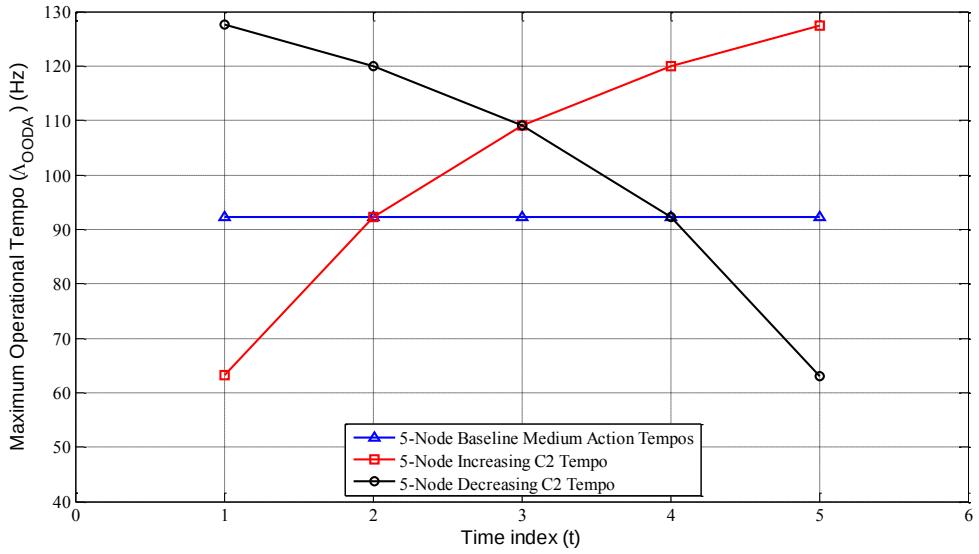

Figure 28. Effects of varying C2 tempo on maximum operational tempo

The results in Figure 28 simulate the gradual increase and decrease of λ_{C2}, but the inference can be made that λ_{C2} could also vary more rapidly in either direction. This would cause an even more drastic change in Λ_{OODA}. The assumption from [6] that every C2 structure has a characteristic decision-making speed is assumed to be correct for the

beginning of any situation. However, the same human-computer interaction may not hold true as the situation unfolds. The human may or may not fully trust the autonomous systems decision-making capability, which causes the decision-making speed to vary. With varying degrees of situations that could be encountered, it is valuable to model autonomous systems at differing rates of decision-making. This would require λ_{C2} to be considered a time-dependent property rather than a top-level property as it currently is.

D. SNR DEPENDENCIES OF DATA THROUGHPUT

In the dynamic scenarios presented, all nodes have the same PAR, packet length, and frame length, which is similar to the parameters employed in the scenario from [12]. The SNR for each link between nodes varies as the dynamic nodes move along their paths, which is due to the range between connecting nodes increasing or decreasing. With this SNR change, there should be a noticeable variation in the data throughput $R_{b\mu}$. In [12], this variation does not occur as expected, and the assumption is because all nodes have the same PAR, packet length, and frame length.

Based on the recommendation from [12], the five-node scenario was modified, by changing these parameters for each node. The only parameters that were changed from the original five nodes were the PAR, packet length, and frame length. The results based on these recommendations did not produce the relationship desired as indicated by [12]. By changing the PAR, packet length, and frame length the data rate of three of the nodes falls below the minimum data rate required for the nodes to assist in generating knowledge for the network. This results in the knowledge function being zero. Although the assumption of changing the PAR, packet length, and frame length does not produce the desired results the original five-node network does. The five-node network is used to display the relationship between SNR and $R_{b\mu}$.

The results of the link based SNR and $R_{b\mu}$ are displayed in side-by-side plots in order to show the relationship between these two parameters. The scale of SNR is in dB, while the scale for $R_{b\mu}$ is in bits-per-second. Figure 29 displays the link based SNR and $R_{b\mu}$ for UAV1. UAV1 is directly connected to three other nodes; therefore it has three

links in the plots. Figure 29 shows that with an increase or decrease in SNR there is an increase or decrease in $R_{b\mu}$ for the links between UAV1 and ATC1, Repeater1, and ATC2. There is variation noticed in each link except the connecting link to ATC1. This is likely due to the minimal SNR variation due to only minor range variation between nodes.

Figure 30 displays the link based SNR and $R_{b\mu}$ for ATC1 for each of the four directly connecting links. Much like UAV1, ATC1, which employs a different modulation scheme, shows the same relationship between SNR and $R_{b\mu}$. The data points reflecting a constant SNR and $R_{b\mu}$ are because the links are between static nodes. The data points reflecting a change in SNR and $R_{b\mu}$ are because the links are between the static node (ATC1), and the two dynamic nodes in the scenario (UAV1 and UAV2). Figure 30 shows that as the SNR decreases between ATC1 and UAV2, the data throughput also decreases. Additionally, the peak in the SNR at time index three is also a peak in $R_{b\mu}$ for the link connecting to UAV1.

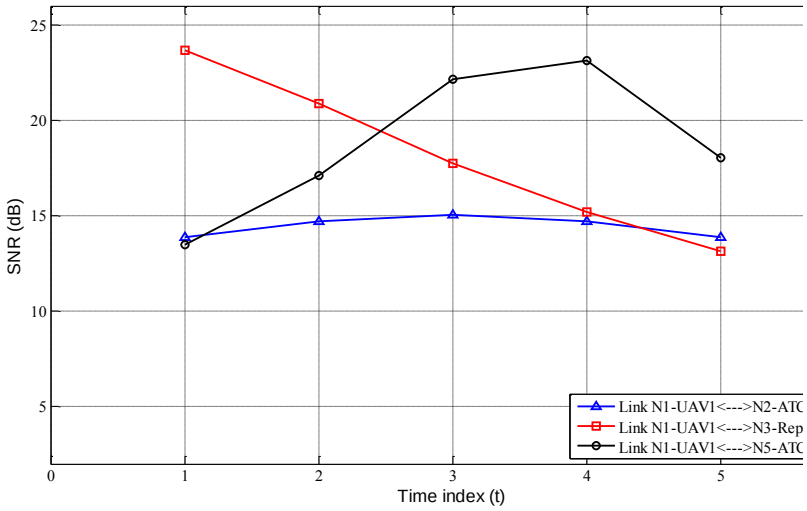

(a)

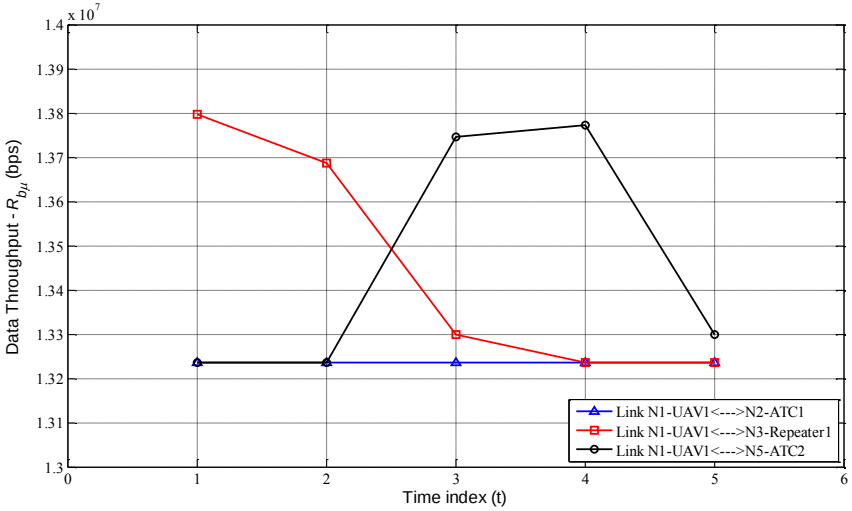

(b)

Figure 29. (a) Link based SNR and (b) Link based $R_{b\mu}$ for UAV1

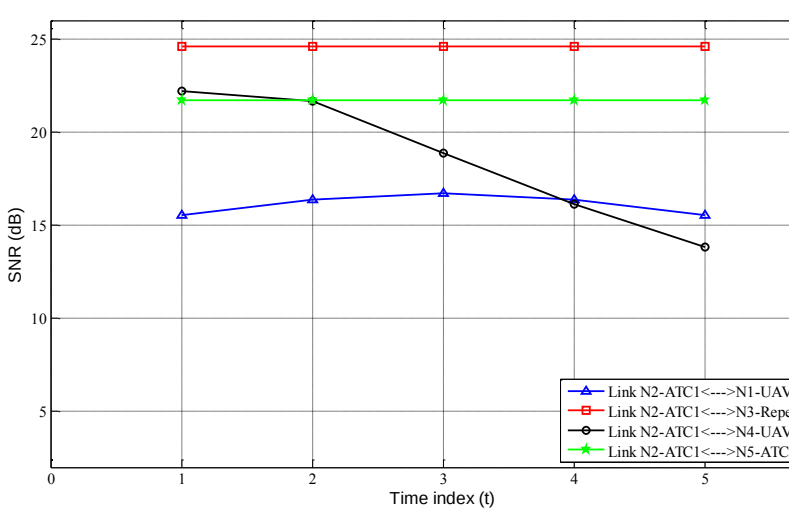

(a)

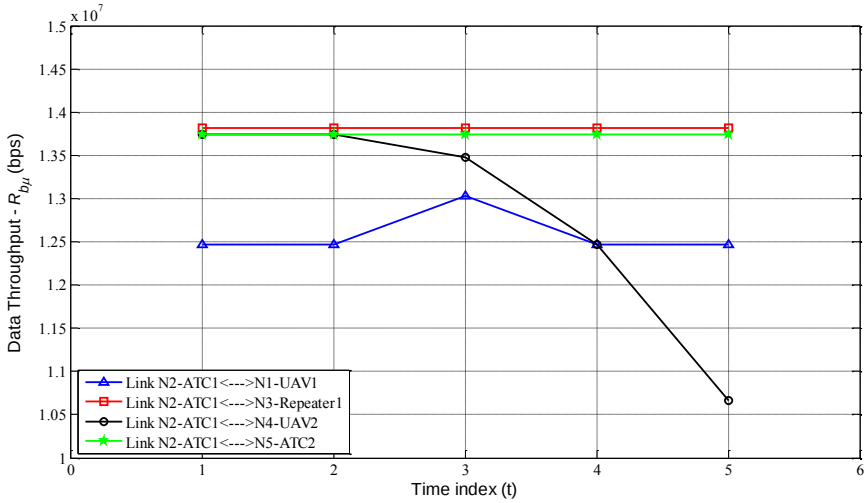

(b)

Figure 30. (a) Link based SNR and (b) Link based $R_{b\mu}$ for ATC1

Figure 31 shows the link based SNR and $R_{b\mu}$ for the four links directly connected to Repeater1. Although Figure 31 shows that all $R_{b\mu}$ values for each time index are 6 Mbps, this is likely due to the modulation scheme (B-PSK) employed by Repeater1 as described in [12]. The maximum data rate for B-PSK is 6 Mbps, and based on the network richness analysis, the knowledge function for Repeater1 is one for all time indexes. This means that the data rate of the node is greater than the maximum data rate allowed to generate knowledge. This forces the data rate of Repeater1 to be limited to the upper bound, which removes the SNR dependency.

Figure 32 displays the link based relationship between SNR and $R_{b\mu}$ for the three links directly connected to UAV2. Much like the link based analysis for UAV1 provided in Figure 29, UAV2 shows similar results. There is a constant decline in both SNR and $R_{b\mu}$ for the link connecting to ATC1 and there is a peak at time index three for the link connecting to ATC2.

Finally, Figure 33 displays the link based SNR and $R_{b\mu}$ relationship for the four links directly connected to ATC2. The constant data points again reflect the links between static nodes, where there is no expected variation, but the links to dynamic nodes show direct correlation as expected. UAV1 is getting closer to ATC2 until time index three, which causes a linear increase in SNR and $R_{b\mu}$, and then a decrease as the range begins to increase again. UAV2 is getting closer ATC2 until time index four, which also causes the increase in SNR and $R_{b\mu}$ as expected, followed by a decrease as range begins to increase after time index four.

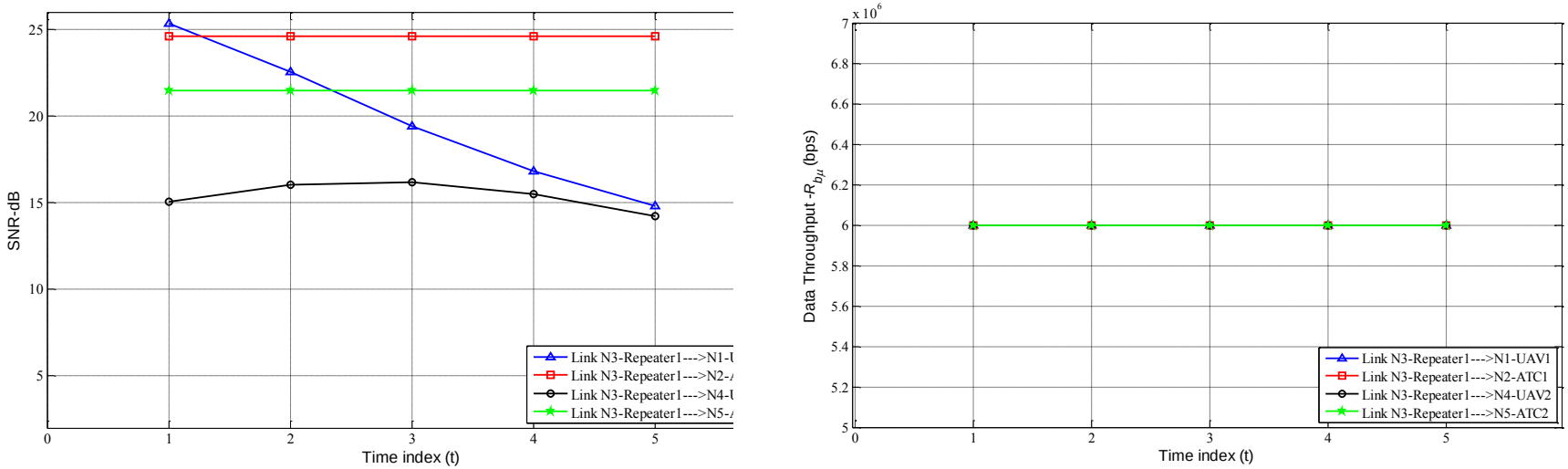

(a) (b)

Figure 31. (a) Link based SNR and (b) Link based $R_{b\mu}$ for Repeater1

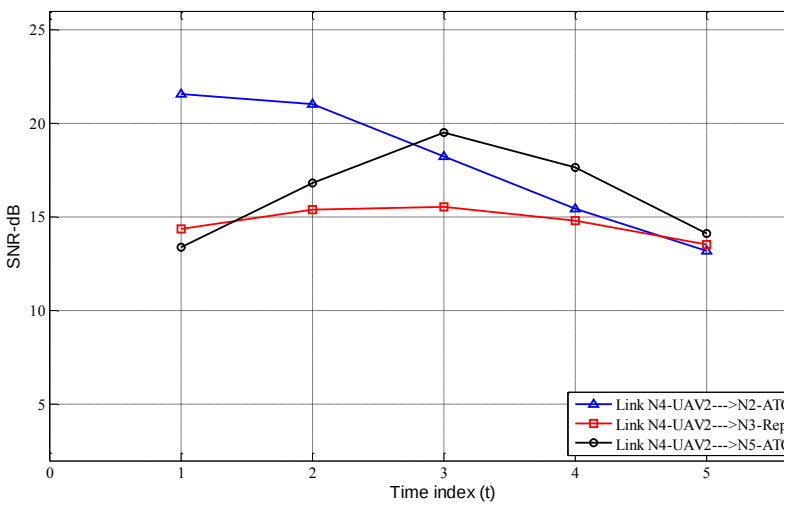

(a)

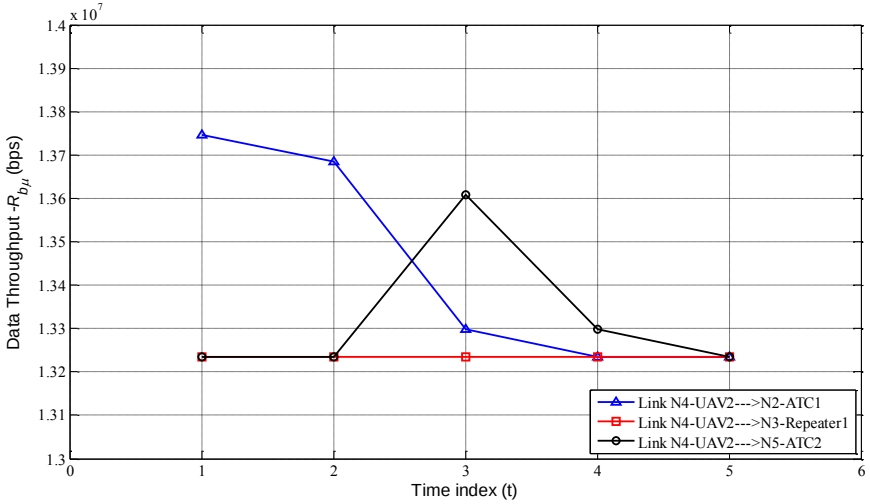

(b)

Figure 32. (a) Link based SNR and (b) Link based $R_{b\mu}$ for UAV2

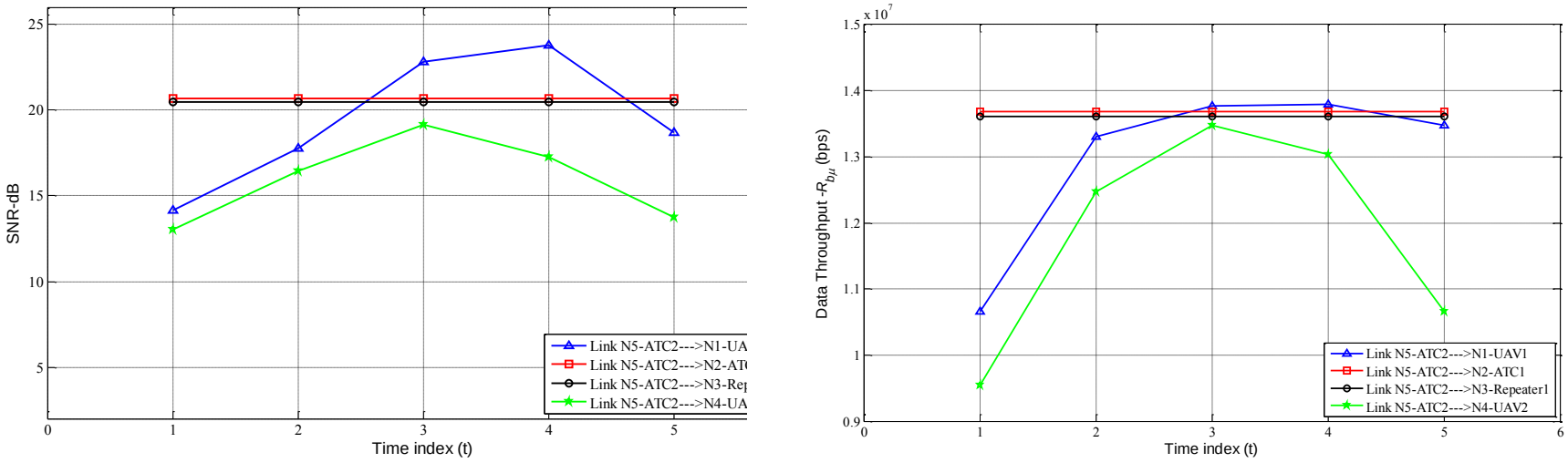

(a) (b)

Figure 33. (a) Link based SNR and (b) Link based $R_{b\mu}$ for ATC2

The results displayed in this section answer the question of the direct relationship between SNR and $R_{b\mu}$. The original results based on the recommended changes indicate that the relationship between SNR and $R_{b\mu}$ is not solely tied to the PAR, packet length, and frame length, but is more a function of whether the minimum data rate is less than the data rate of each node.

E. NETWORK COMPARISON TOOL

LPISimNet(V)2 was not originally designed to conduct network comparison. Generating comparison results requires a laborious process. In order to alleviate the time consuming process of extracting data for comparison, a file is added to LPISimNet(V)3 to plot multiple networks metrics on the same figure. Visual aids often assist in making rapid and informed decisions. A commander does not want to sift through individual numbers to formulate a conclusion about the makeup of the network they want to employ. By providing graphics displaying key network metric comparisons, a commander can make an informed decision without having to do extensive number crunching. The additional file allows for the user to load the simulation results from two different network configurations and plot five specific network metrics which can be used to inform the commander of the best network topology to deploy.

Two dynamic scenarios can be compared, with results being displayed according the specific time index. The user simply types the file extension of the simulation results into the file next to the two load command and selects run on the file. Figures 34 and 35 show an example of the network metric comparison for the characteristic tempo λ_T and maximum operational tempo Λ_{OODA}, for two five node networks.

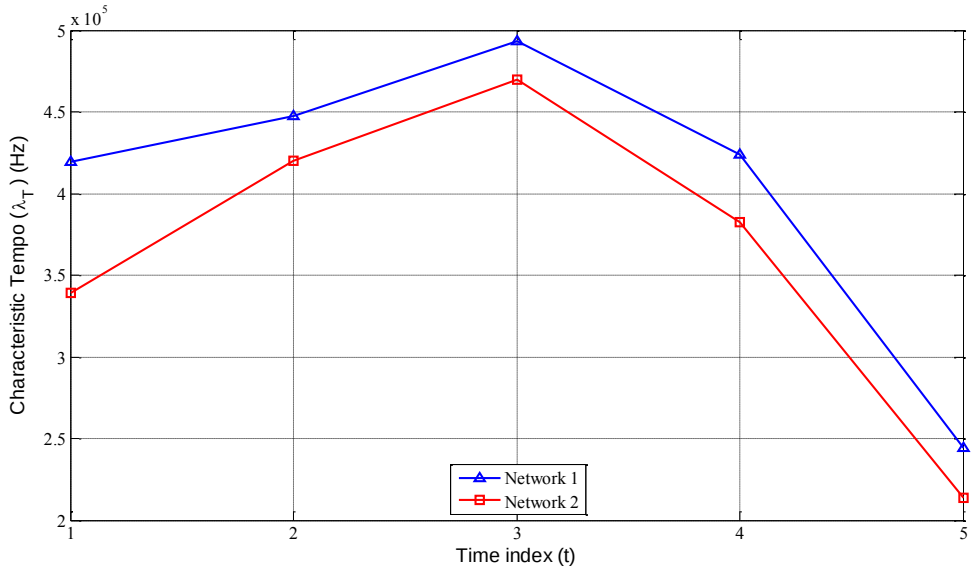

Figure 34. Characteristic tempo comparison example for dynamic networks

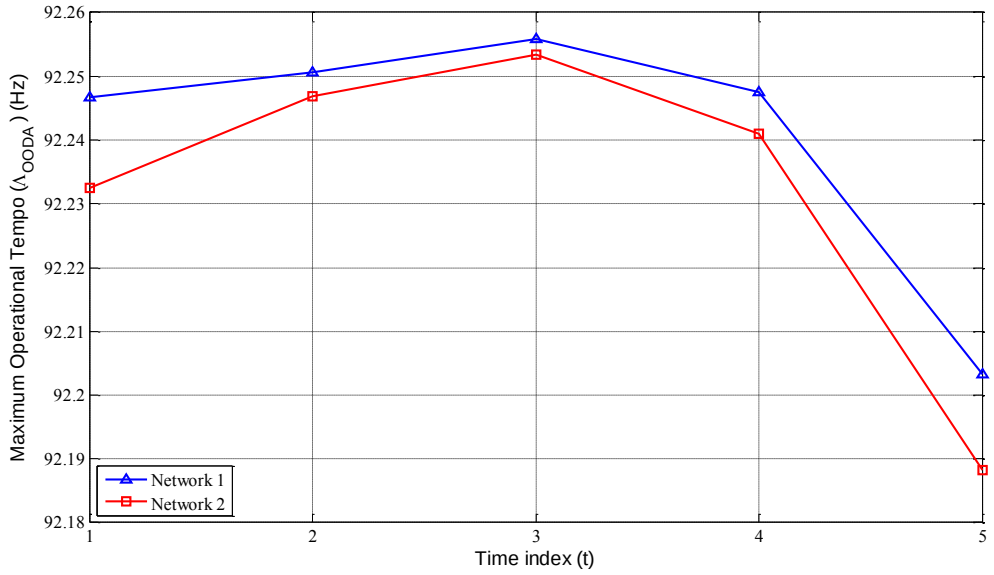

Figure 35. Maximum operational tempo comparison example for dynamic networks

The file will also generate comparison results for connectivity measure, network reach, and network richness. However, the primary metrics to compare are λ_T and Λ_{OODA}. Based on Figures 34 and 35, Network 1's topology is the most beneficial for

sharing information and completing an OODA loop. This ultimately means that Network 1, in this example, would provide the commander with the most efficient network between these two options.

Additionally, static network can be compared in a similar fashion. Due to no time indexes being used for static networks, a bar graph comparison provides an easily understood image for a decision maker. Figures 36 and 37 are provided to show an example comparison of λ_T and Λ_{OODA} for two static networks, where Network 1 is a six node network, and Network 2 is a nine node network.

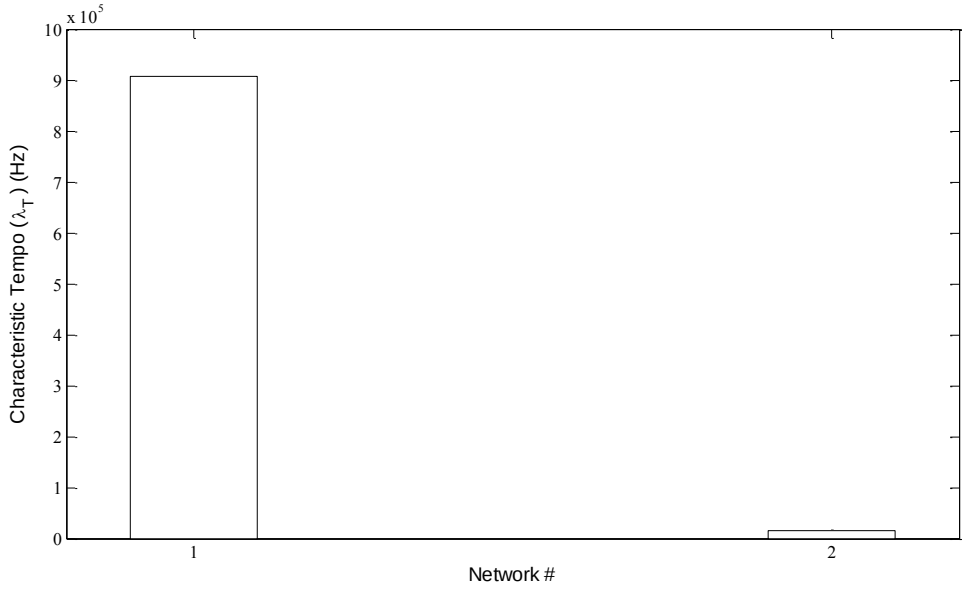

Figure 36. Characteristic tempo comparison example for static networks

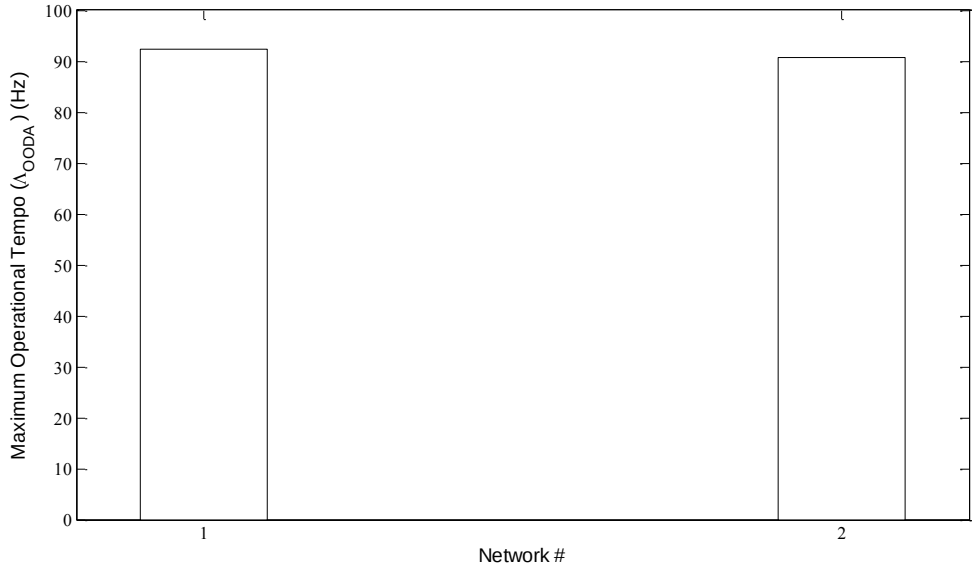

Figure 37. Maximum operational tempo comparison example for static networks

By comparing the static networks utilizing λ_T and Λ_{OODA} it is easy to see that the six node network provides the best solution when considering the rate at which information can be shared and completing an OODA loop. The results of this network comparison tool are just based on examples, but the tool itself would provide a decision-maker with easy to use images to determine which network is best for employment.

This tool could also be used to compare friendly and enemy network capabilities. Command and control doctrine states that in order to be more effective than an opponent, then completing the OODA loop more efficiently is a way to do it [13]. If that is the case for the human decision maker and their force, then it should also translate to the network the force is reliant upon as well. If specific enemy network parameters are known, this tool could also be utilized to compare the friendly versus enemy network in the same manner. This would allow the commander to determine if their network was more efficient than their enemies, which could highlight friendly deficiencies and provide potential vulnerabilities to exploit.

F. CONCLUSION

This chapter substantiated the results of [11] and [12] by showing the results of electronic attack translate directly after additions were made to the model and modifying assumptions presented in recommended future studies. The findings from [11] were supported in that suppressing links within a sensor network reduces the rate at which information can be shared and reduces the overall capability of the network to complete an OODA loop, while also showing the robustness of the network by being able to still exchange information and complete the decision-making cycle.

Next, results were displayed showing that the command and control speed of the network can change as a situation unfolds. This causes a drastic change in the maximum operational tempo of the network. Additionally, the assumption from [12] that changing the PAR, packet length, and frame length will fully display the relationship between SNR and data throughput was found to be incorrect. However, the relationship between SNR and data throughput was displayed for all nodes that are capable of generating knowledge for the network and also do not reach their upper bound for data rate.

Finally, the network comparison tool incorporated into LPISimNet(V)3 was presented. Being able to rapidly display the results of network metrics in graphical form will make the utilization of LPISimNet(V)3 as a network modeling tool easier and more versatile. The next chapter will summarize the findings of this thesis as well as presenting recommendations for future work to further enhance these results.

VI. SUMMARY, RECOMMENDATIONS, AND CONCLUSION

A. SUMMARY

This thesis focused on the effects of network configurations on the characteristic tempo and maximum operational tempo of the network. These results helped highlight important aspects such as network geometry as an important factor to help offset the degradation due to increasing range, as well as point out the fact that the more sensors employed in a network may have adverse effects on the ability of the network to collect and exchange information which is meant to be turned into knowledge. Chapter II focused on reviewing the key network metrics defined in [6], expanding those metrics to include the extended generalized connectivity measure from [8, 11], and describing the adaptive node capability value presented in [7, 12].

Based on the network metrics described in Chapter II, Chapter III provided a description of the network modeling tool LPISimNet(V)3 that is a continuation of the model created originally in [11] and expanded upon in [12]. Chapter III also highlighted difficulties encountered while utilizing LPISimNet(V)2, specifically inaccuracies in the calculation of the knowledge function, along with a correction that was made to make the simulation tool more accurate and leading to the development of LPISimNet(V)3.

Next, Chapter IV provided the basic setup for a static network as it increased in size from two to nine nodes, along with the results of the maximum operational tempo for each static network. Based on the results of the static network, a prediction for future decline of Λ_{OODA} was provided to show how the rate at which the network can complete an OODA loop will continue to degrade as the number of nodes in the network increases. Chapter IV also presented the simulation results for a dynamic scenario, and a potential method for offsetting the decline in λ_T and Λ_{OODA} by increasing C_M. In the dynamic scenario increasing C_M was done by bracketing the dynamic nodes in the network, which allows for the range between static and dynamic nodes to be reduced.

Finally, Chapter V provided validation for practical considerations outlined in [11] by showing the degradation in λ_T and Λ_{OODA} as links are removed from the network due to electronic attack. Also, the new consideration was presented to take into account the possibility of the characteristic decision-making speed of the network changing as a situation dictates. Next, the assumption from [12] that changing the packet arrival rate, packet length, and frame length between nodes will fully display the relationship between SNR and data throughput $R_{b\mu}$ was modified to include the notion that only nodes with data rates greater than the minimum data rate required will display a direct link based relationship between SNR and $R_{b\mu}$, also if a node's data rate is limited by the upper bound then no SNR dependency exists. Side-by-side results for the link based SNR and $R_{b\mu}$ were provided to show the direct correlation between these two parameters holds true for the five-node simulation. Lastly, an additional network comparison tool incorporated into LPISimNet(V)3 was presented. Examples were provided to show the utility of this tool for both dynamic and static scenarios. These results showed that two friendly networks could be compared against each other prior to deployment to determine the most efficient topology, and also could be used to compare friendly and enemy systems to ensure the friendly network was more efficient.

B. BENEFIT TO EXISTING NETWORK ENABLED PROGRAMS

The results of this thesis can provide valuable insight into network solutions being applied to military electronic warfare (EW) programs. Some specific United States Navy and Marine Corps programs are provided in [20] to include Integrated Topside (InTop) and Intrepid Tiger II (IT-2).

The Navy's InTop is designed to help extend the range of the current shipboard EW systems by integrating the ships antennas into a shared EW process [20]. The Marine Corps' IT-2 program consist of network EW pods three different forms of aircraft: UAVs, fixed-wing aircraft, and helicopters [20]. Due to the networked nature of these EW programs, this thesis presents insight in methods to optimize the information exchange capabilities and decision-making cycle involved in deployment and use of these systems.

C. RECOMMENDED FUTURE STUDIES

The future studies to be presented are a result of shortfalls highlighted by using the model or potential future applications of the simulated results.

- Increase the SNR boundaries of LPISimNet(V)3. As noted by the recommendation in [12] the model only accounts for SNR between 13 and 25 dB. Recommend expanding the upper limit of the SNR range above 25 dB. This will allow the users more flexibility in the design of their network while maintaining the minimum requirement typically required by most communication systems of 13 dB.

- Change the command and control tempo λ_{C2} to incorporate the potential for changing the Sheridan Level as time increases throughout a simulation. This will allow for the user to simulate the potential for human interference or a potential increase in autonomy being added as the situation changes. This could be done by removing λ_{C2} from the top level properties of LPISimNet(V)3, and creating a time-dependent properties option, which would vary for each time index simulated.

- Allow for dynamic nodes to change direction during simulations in LPISimNet(V)3. Currently, the program allows only dynamic nodes to move along a straight line path. This would allow for more situations to be modeled, such as convoy routes, or more aviation flight paths. This could again be done by creating a time-dependent properties option, which will allow for the direction of movement to be defined for each time index simulated.

- Modify LPISimNet(V)3 to incorporate parallel processing. This will reduce the computational time, allowing for simulation results to be generated faster. This will also enhance the utility of LPISimNet(V)3 as network modeling tool by being able to model large networks quickly. This will also allow for future studies to validate the prediction presented that the maximum operational tempo will continue to decline as the number of nodes increases. By doing so the maximum number of nodes a network can sustain while still sharing and generating decision-level knowledge could also be predicted with the model.

- Explore solutions for determining accurate values for λ_{C2} if human decision makers are incorporated within the networked system. The rate at which decisions can be made is easy to determine when they are fully automated. The computer will make decisions based on pre-programmed algorithms (input = output). When adding a human decision maker to the system, being able to quantify the rate at which the overall system can make a decision becomes much more difficult.

- Simulate the bracketing method within a swarming system. Swarming technology often includes a large number of sensors collecting and sharing information within an area of interest. Based on the results in Chapter IV, the rate at which information can be shared decreases as the number of sensors increases. If these swarming sensors are bracketed by static collection or C2 nodes, it is assumed that the swarming network will function at a higher rate because C_M can be stabilized.

APPENDIX. CODE CORRECTION LEADING TO LPISIMNET(V)3

There was an error in the MATLAB code in LPISimNet(V)2, which led to inaccurate results for the knowledge function. The error in the code did not allow for the knowledge function to be properly bounded between zero and one but allowed negative numbers. If the knowledge function is a negative value, it will ultimately cause the network richness to be less than it actually is, which also causes the characteristic tempo of the network to appear worse than reality. Figure 38 displays a screen shot of the original code from the CalculatorKu.m file used for one of the modulation schemes in LPISimNet(V)2. All modulation schemes use the same code to compute the knowledge function.

```
Rbmax(NTx,NRx,Ti) = 12e6; %#ok<NASGU>

Node_Lum(NTx,1) = Rbmax(NTx,NRx,Ti) / 2.72; %#ok<NASGU>

if Rb(NTx,NRx,Ti) >= Rbmax(NTx,NRx,Ti)
    Rbmu(NTx,NRx,Ti) = Rbmax(NTx,NRx,Ti); %#ok<AGROW>
else
    Rbmu(NTx,NRx,Ti) = Rb(NTx,NRx,Ti); %#ok<AGROW>
end

Node_Lu(NTx,NRx,Ti) = Rbmu(NTx,NRx,Ti); %#ok<NASGU>
```

Figure 38. Knowledge function code error from LPISimNet(V)2

In Figure 38, the Rbmax value represents the maximum data rate allowed for the modulation scheme. Node_Lum represents the minimum data rate allowed by the hardware of the sensor or communications device being simulated. The error in this code is that there is no argument to specify the minimum value setting where the knowledge function equals zero as specified by equation (5). Figure 37 displays a screen shot of the LPISimNet(V)2 output for the network richness details for the five node dynamic

network used in this thesis. The results show that the knowledge function was computed to be a negative value, which should not be possible.

```
---------------------------
Analysis of Network Richness
---------------------------
Node    Information_Rate    Min_Information_Rate    Knowledge_Function    Information_Rate*Knowledge_Function
1       11332608            13235294.1176           -0.1552               -1758852.7677
2       13443840            8823529.4118            0.4211                5661188.3671
3       6000000             2205882.3529            1.0006                6003791.2818
4       11315712            13235294.1176           -0.15669              -1773113.8592
5       11873664            8823529.4118            0.2969                3525301.3888
Sum( Information_Rate*Knowledge_Function ) = 11658314.4108
Network Richness = 2331662.8822
```

Figure 39. Screen shot of network richness details with incorrect knowledge function results

As it can be seen in Figure 39, the knowledge function for nodes one and four are negative values. According to equation (5), these values should actually be zero, due to the data rate of the hardware being less than the minimum information rate. In order to correct this mistake an additional parameter was added to the code. Figure 40 is a screen shot from CaculatorKu.m with the correction included in LPISimNet(V)3 to account for the lower boundary of the knowledge function.

```
if Rb(NTx,NRx,Ti) < Node_Lum(NTx,1)
    Rbmu(NTx,NRx,Ti) = Node_Lum(NTx,1); %adding a parameter
elseif Rb(NTx,NRx,Ti) >= 2.72*Node_Lum(NTx,1)
    Rbmu(NTx,NRx,Ti)= 2.72*Node_Lum(NTx,1)
else
    Rbmu(NTx,NRx,Ti) = Rb(NTx,NRx,Ti);
end
```

Figure 40. Corrected knowledge function code for LPISimNet(V)3

The primary addition was the inclusion of the first if category to the code. This causes the computation to account for the zero condition established by (6). Figure 41 provides a screen shot of the network richness details after the code was modified to for the exact same network simulation.

```
----------------------------
Analysis of Network Richness
----------------------------
Node   Information_Rate   Min_Information_Rate   Knowledge_Function   Information_Rate*Knowledge_Function
1      13422313.4118      13235294.1176          0.014031             188334.4379
2      13443840           8823529.4118           0.4211               5661188.3671
3      6000000            2205882.3529           1.0006               6003791.2818
4      13405417.4118      13235294.1176          0.012772             171212.0014
5      11873664           8823529.4118           0.2969               3525301.3888
Sum( Information_Rate*Knowledge_Function ) = 15549827.477
Network Richness = 3109965.4954
```

Figure 41. Screen shot of network richness details with correct knowledge function results

As Figure 41 displays, the knowledge function for both node one and four is approximately zero. In order to show that the knowledge function is actually accounting for the zero case in the minimum information rate for the M-QAM modulation scheme was modified to be greater than the minimum information rate for the nodes employing the M-QAM modulation scheme. Figure 42 displays a screen shot of the network richness details after the minimum information rate modification was made.

```
----------------------------
Analysis of Network Richness
----------------------------
Node   Information_Rate   Min_Information_Rate   Knowledge_Function   Information_Rate*Knowledge_Function
1      37700000           37700000               0                    0
2      13443840           8823529.4118           0.4211               5661188.3671
3      6000000            2205882.3529           1.0006               6003791.2818
4      37700000           37700000               0                    0
5      11873664           8823529.4118           0.2969               3525301.3888
Sum( Information_Rate*Knowledge_Function ) = 15190281.0377
Network Richness = 3038056.2075
>>
```

Figure 42. Screen shot of network richness details with modified minimum information rate to show correct knowledge function results

It is shown by Figure 42 that the zero condition is met by the modified knowledge function code. The information rate of the hardware was below the minimum information rate required. With the modification to the code, the information rate was forced to be the minimum; therefore nodes one and four no longer provide knowledge to the network. The results in Figure 42 are only for the demonstration of the code. These results were not used in the actual simulations.

THIS PAGE INTENTIONALLY LEFT BLANK

LIST OF REFERENCES

[1] P. W. Singer. *Wired for War*. New York: Penguin Press, 2009, pp. 179–180.

[2] P. E. Pace. *Detecting and Classifying Low Probability of Intercept Radar.* Boston: Artech House, 2009.

[3] P. W. Phister and J. D. Cherry. "Command and control concepts within the network-centric operations construct," in *IEEE Aerosp. Conf.*, Big Sky, MT, 2006.

[4] *Marine Air Ground Task Force Information Operations*, MCWP 3-40.4, USMC, Quantico, VA, 2013, pp. 1-2 – 1-3.

[5] S. Elson and D. Estrin, "Sensor Networks: A Bridge to the Physical World," in *Wireless Sensor Networks*. New York: Springer, 2004, ch. 1, pp 3–13.

[6] M. F. Ling, T. Moon, and E Kruzins, "Proposed network centric warfare metrics: From connectivity to the OODA cycle," *Military Operations Research,* vol. 10, no. 1, pp. 5–13, 2005.

[7] M. V. Magalhaes, T. E. Smith, and P. E. Pace, "Adaptive node capability to assess the characteristic tempo in a distributed communication network," in *IEEE Wireless Comm. and Networking Conf. 2012*, Paris, France, 2012, pp. 3040 – 3045.

[8] Y. Chen and P. E. Pace, "Simulation of information metrics to assess the value of networking in a general battlespace topology," in *IEEE Sys. of Sys. Eng. 2008*, Monterey, CA, 2008.

[9] J. Sheu, G. Chang, and Y. Chen, "A novel approach for k-coverage rate evaluation and re-deployment in wireless sensor networks," in *IEEE Global Telecomm. Conf. 2008.* New Orleans, LA, 2008, pp. 341–345.

[10] R. Savani, "High-frequency trading: The faster, the better?" *IEEE Intelligent Systems,* vol. 27, no. 4, pp. 70–73, July–Aug. 2012.

[11] Y. Chen, "Simulation of network-enabled electronic warfare metrics to assess the value of networking in a general information and radar topology," M.S. thesis, Dept. of Info. Sciences, Naval Postgraduate School, Monterey, CA, 2007.

[12] M. V. Magalhaes, "Adaptive node capability metric to assess the value of networking in a general command and control wireless communication topology," M.S. thesis, Dept. of Info. Sciences, Naval Postgraduate School, Monterey, CA, 2011.

[13] *Command and Control*, MCDP-6, USMC, Quantico, VA, pp. 63–65, 1996.

[14] Q. Liu, S. Zhou and G. Giannakis, "Queuing with adaptive modulation and coding over wireless links: Cross-layer analysis and design," *IEEE Trans. on Wireless Comm.*, vol. 4, no. 3, pp. 1142–1153, May 2005.

[15] Q. Liu, S. Zhou and G. Giannakis, "Cross-layer modeling of adaptive wireless links for QoS support in heterogeneous wired-wireless networks," *Wireless Networks*, vol. 12, no. 4, pp. 427–437, Jul. 2006.

[16] B. Sklar, "Communications Link Analysis," in *Digital Communications Fundamentals and Applications*, Englewood Cliffs, NJ: Prentice-Hall, 1988, ch. 4, sec. 4.4.1, pp. 205–206.

[17] *Remote Sensor Operations*, MCWP 2-15.1, USMC, Quantico, VA, pp. B-3, 1997.

[18] R. Kershner, "The number of circles covering a set," in *American Journal of Mathematics*, vol. 61, pp. 665–671, 1939.

[19] D. Xuan, "Connected coverage of wireless networks in theoretical and practical settings," PowerPoint Presentation, The Ohio State University, May 2010 [Online]. Available: http://www.cse.ohiostate.edu/~xuan/RP/xuan_connected_coverage.ppt.

[20] J. Wilson, "Electronic warfare to be part of all military operations," in *Military and Aerospace Electronics*, vol. 25, no. 8, pp. 8–17, Aug. 2014.

INITIAL DISTRIBUTION LIST

1. Defense Technical Information Center
   Ft. Belvoir, Virginia

2. Dudley Knox Library
   Naval Postgraduate School
   Monterey, California